



# $^{53}\text{Mn}$ – $^{53}\text{Cr}$ radiometric dating of secondary carbonates in CR chondrites: Timescales for parent body aqueous alteration

Christine E. Jilly-Rehak<sup>a,b,\*</sup>, Gary R. Huss<sup>b</sup>, Kazuhide Nagashima<sup>b</sup>

<sup>a</sup> Department of Geology and Geophysics, University of Hawai'i at Mānoa, 1680 East-West Road, POST 701, Honolulu, HI 96822, USA

<sup>b</sup> Hawai'i Institute of Geophysics and Planetology, University of Hawai'i at Mānoa, 1680 East-West Road, POST 602, Honolulu, HI 96822, USA

Received 24 February 2016; accepted in revised form 27 August 2016; available online xxx

## Abstract

We present  $^{53}\text{Mn}$ – $^{53}\text{Cr}$  ages of secondary carbonates in Renazzo-like (CR) chondrites, determined by secondary ion mass spectrometry. The timing of aqueous alteration in CR chondrites has been unconstrained in the literature. We measured  $^{53}\text{Mn}$ – $^{53}\text{Cr}$  isotope systematics in carbonates from three different CR-chondrite lithologies. Calcite in the interchondrule matrix of Renazzo, calcite in the matrix of GRO 95577, and dolomite in a dark inclusion of Renazzo all show excesses in  $^{53}\text{Cr}$ , interpreted as the daughter product from the decay of  $^{53}\text{Mn}$ . The Renazzo calcite yields an initial ratio of  $(^{53}\text{Mn}/^{55}\text{Mn})_0 = (3.6 \pm 2.7) \times 10^{-6}$ , and the Renazzo dark inclusion dolomite ranges from  $(^{53}\text{Mn}/^{55}\text{Mn})_0 = (3.1 \pm 1.4) \times 10^{-6}$  (corrected to the RSF of a calcite standard) to  $(3.7 \pm 1.7) \times 10^{-6}$  (corrected to an inferred dolomite RSF). When anchored to the D'Orbigny angrite, the Renazzo carbonates yield ages between 4563.6 and 4562.6 Ma, or  $\sim 4.3$ – $5.3$  Myr after the formation of CV CAIs. Calcite measured in the heavily altered specimen GRO 95577 yields a shallower slope of  $(^{53}\text{Mn}/^{55}\text{Mn})_0 = (7.9 \pm 2.8) \times 10^{-7}$ , corresponding to a much younger age of 4555.4 Ma, or  $\sim 12.6$  Myr after CAI formation. The two Renazzo ages are contemporaneous with Mn–Cr ages of carbonates in Tagish Lake, CI, and CM chondrites, but the GRO 95577 age is uniquely young. These findings suggest that early aqueous alteration on chondritic parent bodies was a common occurrence, likely driven by internal heating from  $^{26}\text{Al}$  decay after accretion. The young carbonate ages of GRO 95577 suggest that either the CR parent body was sufficiently large to sustain heating from  $^{26}\text{Al}$  for  $\sim 8$  Myr, or that late-stage impact events supplied heat to the region where GRO 95577 originated.

© 2016 Elsevier Ltd. All rights reserved.

**Keywords:** Radiometric dating; Chondrites; Carbonaceous chondrites; Aqueous alteration; Meteoritics; Secondary processes

## 1. INTRODUCTION

The Renazzo-like (CR) carbonaceous chondrites are useful for the study of aqueous alteration, as the lithologies can range from nearly anhydrous to completely hydrated, with most samples being partially altered (Weisberg et al., 1993; Kallemeyn et al., 1994; Weisberg and Huber 2007; Abreu

and Brearley 2010; Schrader et al., 2011; Harju et al., 2014). These various stages of hydration show the process of alteration, revealing how elements were transported in the fluid (e.g., Burger and Brearley, 2004), and can be used to understand the water–rock reactions that formed the secondary minerals (e.g., Weisberg et al., 1993; Clayton and Mayeda, 1999). The secondary mineralogy in CR chondrites has been documented in literature, with the most significant alteration products being serpentine minerals, clays, Fe, Ni-bearing sulfides, magnetite, and carbonates (e.g., Brearley, 2006, and references therein). Though the petrographic context of CR aqueous alteration has been described, many questions remain regarding the timescales of alteration.

\* Corresponding author at: Space Sciences Lab, 7 Gauss Way, Berkeley, CA 94720, USA.

E-mail addresses: [jillyrehak@ssl.berkeley.edu](mailto:jillyrehak@ssl.berkeley.edu) (C.E. Jilly-Rehak), [ghuss@higp.hawaii.edu](mailto:ghuss@higp.hawaii.edu) (G.R. Huss), [kazu@higp.hawaii.edu](mailto:kazu@higp.hawaii.edu) (K. Nagashima).

<http://dx.doi.org/10.1016/j.gca.2016.08.033>

0016-7037/© 2016 Elsevier Ltd. All rights reserved.

The  $^{53}\text{Mn}$ – $^{53}\text{Cr}$  system is a robust radiochronometer for dating the formation of early solar system materials. Radioactive  $^{53}\text{Mn}$  decays into stable  $^{53}\text{Cr}$  via electron capture. This process has a half-life of  $3.7 \pm 0.4$  Myr (Honda and Imamura, 1971), long enough to date minerals that were formed during the first  $\sim 20$  Myr of Solar System history (e.g., Lugmair and Shukolyukov, 1998; Shukolyukov and Lugmair, 2006). The ages of aqueous alteration events in Ivuna-like (CI), Mighei-like (CM), and Vigarano-like (CV) chondrites have been estimated to range from 1 to 15 Myr after the formation of Ca–Al-rich inclusions (CAIs), the first Solar System solids (e.g., Krot et al., 2006a). These ages were based on  $^{53}\text{Mn}$ – $^{53}\text{Cr}$  measurements of carbonates, as well as  $^{129}\text{I}$ – $^{129}\text{Xe}$  measurements of magnetite and phyllosilicates. Carbonates can yield precise secondary ages from  $^{53}\text{Mn}$ – $^{53}\text{Cr}$  dating as they fractionate Mn and Cr during formation from aqueous fluids. However, many of the reported carbonate  $^{53}\text{Mn}$ – $^{53}\text{Cr}$  ages were based upon incorrect assumptions about mineral relative sensitivity factors, inadequate time anchors, and poorly defined solar-system initial  $^{53}\text{Mn}/^{55}\text{Mn}$  ratios (see discussion below), stressing the need for more accurate and consistent analyses.

There is a lack of knowledge about the timing of secondary alteration in CR chondrites as compared to other chondrite groups. Literature studies of radiometric  $^{53}\text{Mn}$ – $^{53}\text{Cr}$  dating of secondary minerals have been dominated by studies of the CI and CM chondrites, where carbonate minerals are more abundant and coarse-grained, hence easier to target and measure (e.g., Endreß et al., 1996; Hoppe et al., 2007; De Leuw et al., 2009; Petitat et al., 2009, 2011; Blinova et al., 2012; Lee et al., 2012; Fujiya et al., 2012, 2013). Secondary fayalite grains have been measured for  $^{53}\text{Mn}$ – $^{53}\text{Cr}$  dating in CV, Ornans-like (CO), and unequilibrated ordinary chondrites, in which carbonates are virtually absent (e.g., Hutcheon et al., 1998; Hua et al., 2005; Jogo et al., 2009; Doyle et al., 2015). Fayalite has not been found in CR chondrites, and most of the carbonate material exists as fine-grained masses intergrown with matrix phyllosilicates, unsuitable for *in situ* measurement. For accurate analysis, it is important that the target mineral consists of only one phase, and is free of inclusions that may contain different isotopic compositions. Only one study has attempted to measure CR-chondrite alteration ages by looking at  $^{53}\text{Mn}$ – $^{53}\text{Cr}$  in siderite (Tyra et al., 2010). They did not find resolved excesses of radiogenic  $^{53}\text{Cr}$  and suggested that aqueous alteration persisted until after the majority of  $^{53}\text{Mn}$  had decayed,  $>20$  Myr after CAI formation.

An accurate timescale for aqueous alteration of CR chondrites can provide a critical constraint on the location of alteration and the heat source for melting of water ice. It is generally agreed from petrographic and isotopic observations that most aqueous alteration processes occurred on the asteroidal parent body after accretion (Weisberg et al., 1993; Burger and Brearley, 2004; Brearley, 2006; Weisberg and Huber, 2007; Schrader et al., 2011, 2014; Abreu and Bullock, 2013); however, it has also been argued that some alteration features observed in chondrites were formed before the final assembly of the meteorite parent

bodies (e.g., Ichikawa and Ikeda, 1995; Weisberg and Prinz, 1998). According to asteroidal models of alteration, secondary minerals were formed on the parent body due to the interaction between primitive chondritic rock and liquid water (McSween, 1979; Weisberg et al., 1993; Browning et al., 1996; Clayton and Mayeda, 1999; Jogo et al., 2009). These models require a source of heat to melt the accreted ice on the asteroidal parent body, usually credited to internal  $^{26}\text{Al}$ -decay or external impact heating (e.g., Abreu and Bullock, 2013). In an internal heating scenario, the aqueous alteration would necessarily occur after chondrule formation (chondritic asteroids cannot form until there are chondrules), but not so late as to escape heating on the parent body from  $^{26}\text{Al}$ . External heating from impacts can account for late-stage parent body alteration ages.

Models of pre-accretionary aqueous alteration posit that hydrous minerals could have formed through the reaction of anhydrous nebular phases and water vapor as the solar nebula cooled (Cyr et al., 1998), or during the passage of shock waves in an ice-enriched region of the solar nebula (Ciesla et al., 2003). The solar disk is thought to have dissipated within  $\sim 5$  Myr after CAI formation (Cyr et al., 1998; Brearley, 2006), consistent with observations of young stellar objects in clusters in our galaxy where nearly all have lost their disks by 6 Myr (Haisch et al., 2001). Chondritic parent bodies accreted perhaps as early as about 2 Myr and no later than 3–4 Myr after CAI formation (Cohen and Coker, 2000). Thus, secondary mineral ages less than  $\sim 2$ –3 Myr after CAI formation could potentially support pre-accretionary models, while alteration occurring over 4 Myr after CAI formation would favor an asteroidal setting for alteration.

In this study, two CR chondrites, Renazzo and Grosvenor Mountains (GRO) 95577, were found to have coarse-grained carbonates large enough (greater than  $\sim 10$   $\mu\text{m}$ ) to measure with secondary ion mass spectrometry (SIMS). We present resolved  $^{53}\text{Mn}$ – $^{53}\text{Cr}$  ages of aqueously produced calcite and dolomite. We describe the mineralogy and petrology of the secondary carbonates, detailing the observed crystal morphologies. The methods for measuring  $^{53}\text{Mn}$ – $^{53}\text{Cr}$  systematics by SIMS are discussed, including a description of relative sensitivity factors and associated uncertainties. This study places important constraints on the timing and nature of the aqueous alteration process for CR chondrites, and has broader implications regarding the heat sources required for alteration to occur.

## 2. ANALYTICAL METHODS

### 2.1. Thin section mineralogy and petrography

A total of three sections from the two meteorites Renazzo and GRO 95577 were used in this work (Table 1). All three thin sections were made without water to minimize aqueous alteration and oxidation during sample preparation. All thin sections were initially observed and characterized using optical microscopy. After carbon-coating, element X-ray maps of each thin section were obtained using the JEOL JXA-8500F field-emission electron microprobe at the University of Hawai'i. Ca, Fe,

Table 1  
Samples of CR chondrites used in this study.

Meteorite <sup>a</sup>	Petrologic type <sup>b</sup>	Fall/find	Weathering grade
GRO 95577,69	CR 2.0	Find	B
Renazzo NHMW-N1126	CR 2.4	Fall	N/A
Renazzo NHMW-N1127	CR 2.4	Fall	N/A

<sup>a</sup> GRO 95577,69 section made at Johnson Space Center, Renazzo N1126 and N1127 made at Museum of Natural History Vienna, for the purpose of this study.

<sup>b</sup> Petrologic types as defined in Harju et al. (2014).

Mg, Al, and S were measured using a 50 nA beam at 15.0 kV. Individual elemental maps were combined into multi-element pseudo-mineral maps, which were used to identify potential carbonate-rich regions for ion microprobe measurements. Sections were also imaged using backscattered-electron (BSE) imaging on a JEOL JSM 5900LV scanning electron microscope (SEM) set to an accelerating voltage of 15 kV. Carbonate grains for Mn–Cr isotope analysis were identified using semi-quantitative energy dispersive X-ray spectroscopy (EDX).

Quantitative X-ray spot analyses of standards and carbonate grains in Renazzo and GRO 95577 were made using the electron microprobe after SIMS, using methods similar to those of Jilly et al. (2014). Elements Mn, Cr, Ca, Mg, and Si were measured at an accelerating voltage of 15 kV for 30 s each. For dolomite analyses, Fe was also measured. Since carbonates are susceptible to electron beam damage and outgassing during analysis, measurements were taken at 10 nA, with an 8- $\mu$ m-diameter beam for the Sugiura calcite standards, and a 1- $\mu$ m beam for meteoritic carbonates. Detection limits (in elemental weight percent) were 0.04, 0.03, 0.03, 0.02, 0.02, and 0.01 for Mn, Cr, Fe, Ca, Mg, and Si, respectively. EPMA standards included terrestrial garnet, chromite, San Carlos olivine, calcite, and dolomite. The carbon content was calculated stoichiometrically relative to cations by assuming that there are 0.333 atoms of C per atom of O. The EPMA procedure for measuring the San Carlos olivine standard was optimized for detecting trace elements in olivine, measured with a 10- $\mu$ m beam at 15 kV and a current of 100 nA. Detection limits were 0.008, 0.005, 0.014, 0.003, 0.002, and 0.002 for Mn, Cr, Fe, Ca, Mg, and Si, respectively. The standards included terrestrial Fe-rich olivine, diopside, chromite, and San Carlos olivine.

## 2.2. Secondary ion mass spectrometry (SIMS)

Carbonates in the three CR chondrite thin sections were measured for Mn abundance and Cr isotopes using SIMS on the University of Hawai'i Cameca ims 1280 ion microprobe. Two calcite grains were measured from the Renazzo N1127 matrix, five calcite grains from the GRO 95577 matrix, and seven dolomite grains from a dark inclusion from Renazzo N1126. All calcite measurements were made during a single session, and the dolomite was analyzed during a second session using very similar analytical conditions, and procedures similar to those described by Jilly et al. (2014). Measurements used the duoplasmatron  $^{16}\text{O}^-$  source with a  $\sim$ 100 pA primary beam focused to  $\sim$ 5  $\mu$ m

in diameter (no raster).  $^{52}\text{Cr}^+$  and  $^{53}\text{Cr}^+$  were measured in multi-collection mode (45 s) followed by a peak jump to  $^{55}\text{Mn}^+$  (2 s). All isotopes were measured by electron multipliers, and a typical measurement consisted of  $\sim$ 100 cycles. The mass-resolving power was  $\sim$ 4800 for  $^{52}\text{Cr}^+$ , and was  $\sim$ 6500 for  $^{53}\text{Cr}^+$  and  $^{55}\text{Mn}^+$  to resolve the interference from  $^{52}\text{CrH}^+$  on  $^{53}\text{Cr}^+$ . Calcite grains were pre-sputtered for 600 s using a  $\sim$ 300 pA beam and 5  $\mu\text{m} \times 5 \mu\text{m}$  raster, and dolomite grains were pre-sputtered for 360 s at  $\sim$ 100 pA with no raster, to remove carbon coating and surface contamination. Synthetic Mn- and Cr-bearing calcites provided by N. Sugiura from the University of Tokyo (Sugiura et al., 2010) and San Carlos olivine were used as standards.

After measurement, the raw data were read into an in-house data-reduction package. The isotope ratios were calculated using the sum of the total counts, rather than the mean of the ratios, to reduce statistical bias due to low count rates (Ogliore et al., 2011). The uncertainties on  $^{55}\text{Mn}/^{52}\text{Cr}$  represent the statistical uncertainty combined with the uncertainties in the relative sensitivity factors (cf. Section 2.3. below), which accounts for non-statistical variation in the  $^{55}\text{Mn}/^{52}\text{Cr}$  ratio. In addition, the  $^{55}\text{Mn}/^{52}\text{Cr}$  ratios can vary within a single carbonate grain due to trace element zoning or individual crystal growths incorporating different amounts of Mn and Cr. In some cases, the data from one grain was split into multiple points if it appeared that we sampled zoning in  $^{55}\text{Mn}/^{52}\text{Cr}$ . The criteria for splitting an analysis was if the  $^{55}\text{Mn}/^{52}\text{Cr}$  ratio over time exhibited plateaus, i.e., the ratio was steady at one value, then jumped to another significantly different value and was steady there for at least  $\sim$ 15 cycles. This method was used to avoid averaging over a very wide  $^{55}\text{Mn}/^{52}\text{Cr}$  distribution, which would introduce correlated error in the measurement. Caution must be taken when splitting data, as it can re-introduce ratio bias if the total counts are sufficiently low; for our worst-case scenario the total counts in the ratio denominator was 800, which corresponds to a maximum possible bias of  $\sim$ 1‰ in the  $^{53}\text{Cr}/^{52}\text{Cr}$  ratio (Ogliore et al., 2011).

To provide a conservative estimate of the uncertainties on  $^{53}\text{Cr}/^{52}\text{Cr}$ , we use 2 times the standard error of the measured ratios (i.e., the standard deviation divided by the square root of N), since the purely statistical uncertainties are likely an underestimate of the total error. The sample data were corrected for instrumental mass fractionation externally using the mean  $^{53}\text{Cr}^+/^{52}\text{Cr}^+$  ratios measured in the standards compared to the reference ratio of  $^{53}\text{Cr}/^{52}\text{Cr} = 0.113459 \pm 0.000005$  (Papanastassiou, 1986).

The  $^{53}\text{Cr}^+ / ^{52}\text{Cr}^+$  ratios for the standards were consistent throughout the measurement, with precisions of 3.6‰ (two standard deviations) in San Carlos olivine, and 2.7‰ in the synthetic calcite standard (standard data presented in [supplemental material](#)). These values were propagated into the total uncertainty for the meteorite  $^{53}\text{Cr} / ^{52}\text{Cr}$  analyses. We could not use  $^{50}\text{Cr}^+ / ^{52}\text{Cr}^+$  to make an internal instrumental-mass-fractionation correction, because the interferences from  $^{50}\text{V}^+$  and  $^{50}\text{Ti}^+$  on  $^{50}\text{Cr}^+$  were too large. The  $^{53}\text{Cr}$  excesses in the unknowns are reported as  $\delta^{53}\text{Cr}^*$  in units of per mil (Eq. (1)).

$$\delta^{53}\text{Cr}^* = \left[ \left( \frac{^{53}\text{Cr}^+ / ^{52}\text{Cr}^+}{\text{IMF-corrected}} / 0.113459 \right) - 1 \right] \times 1000 \quad (1)$$

### 2.3. $^{55}\text{Mn} / ^{52}\text{Cr}$ relative sensitivity factors

One of the largest – and most difficult to constrain – sources of error to consider during Mn–Cr measurements by SIMS is the relative sensitivity factor (RSF). The RSF describes the relative efficiency with which ions of different elements sputtered from the sample are transferred to the detectors. We define the RSF as:

$$\text{RSF} = \left[ \frac{^{55}\text{Mn}^+ / ^{52}\text{Cr}^+}{\text{SIMS}} / \left( \frac{^{55}\text{Mn} / ^{52}\text{Cr}}{\text{TRUE}} \right) \right] \quad (2)$$

The RSF is determined using SIMS and EPMA data for the standards. It should be noted that in some studies, the RSF value has been defined using the inverse of the ratio in Eq. (2) ([McKibbin et al., 2013, 2015](#); [Steele and McKeegan, 2014](#)). To quantify the real  $^{55}\text{Mn} / ^{52}\text{Cr}$  value of the meteoritic carbonates, we divide the  $(^{55}\text{Mn}^+ / ^{52}\text{Cr}^+)$  measured by SIMS by our RSF.

The  $^{53}\text{Mn}$ – $^{53}\text{Cr}$  dating of carbonates has historically been standardized to silicates. Carbonates that contain measurable amounts of both Cr and Mn are extremely rare on Earth and are difficult to synthesize, as the carbonate structure does not accommodate the  $\text{Cr}^{2+}$  ion, and  $\text{Cr}^{2+}$  readily oxidizes in the presence of water. Although earlier workers knew that matrix effects could change the RSF, the lack of adequate carbonate standards led to the widespread use of silicate standards for consistency (e.g., [Hoppe et al., 2007](#); [De Leuw et al., 2009](#); [Petitat et al., 2011](#); [Lee et al., 2012](#)). Mn- and Cr-bearing carbonates have recently been synthesized ([Sugiura et al., 2010](#); [Ichimura and Sugiura, 2015](#)), allowing the variation in the Mn–Cr RSF between carbonates and silicates to be measured. There is now solid evidence that the  $^{55}\text{Mn} / ^{52}\text{Cr}$  ratio and hence  $^{53}\text{Mn}$ – $^{53}\text{Cr}$  ages of many previous studies were inaccurately determined, because the Mg-rich silicate standards used were unlike the analyzed materials ([Sugiura et al., 2010](#); [Fujiya et al., 2012, 2013](#); [McKibbin et al., 2013](#); [Steele and McKeegan, 2014](#); [Ichimura and Sugiura, 2015](#); [Doyle et al., 2016](#)). Therefore, numerous grains of the synthetic Mn and Cr calcite prepared by N. Sugiura and W. Fujiya were provided to the University of Hawai'i as standards for  $^{53}\text{Mn}$ – $^{53}\text{Cr}$  dating.

The synthetic calcites are radially zoned in both Mn and Cr content, and therefore the  $^{55}\text{Mn} / ^{52}\text{Cr}$  composition cannot be defined as a single value for the entire standard.

For this reason, SIMS spots were targeted in a small region on the standard to avoid chemical zoning. The  $(^{55}\text{Mn}^+ / ^{52}\text{Cr}^+)_{\text{SIMS}}$  ratios were sufficiently homogeneous, with an average composition of  $0.68 \pm 0.06$  ( $2\sigma$  standard deviation, see [supplemental material](#)). After SIMS analysis, we determined the  $(^{55}\text{Mn} / ^{52}\text{Cr})_{\text{TRUE}}$  values for the synthetic calcite standards using EPMA, by targeting multiple points surrounding each SIMS pit. The EPMA measurements (four per SIMS pit) were averaged to obtain a Mn/Cr abundance ratio for each SIMS standard analysis. Since zoning in the standard occurs on a scale smaller than the electron beam, this method introduces additional uncertainty into the EPMA data. While this calcite standard is not perfect, it is currently the best option for constraining the true RSF for carbonates.

To calculate the RSF, the isotopic  $^{52}\text{Cr}$  abundance of 0.83785 ([Papanastassiou, 1986](#)) was multiplied by the atomic abundance of Cr determined by EPMA. No isotopic correction factor is needed for  $^{55}\text{Mn}$ , as it is the only stable isotope of Mn. Each value of  $(^{55}\text{Mn} / ^{52}\text{Cr})_{\text{TRUE}}$  was then ratioed to the corresponding standard SIMS measurement. The uncertainty was determined by combining the statistical uncertainty from counting statistics in the SIMS measurements with standard deviation of EPMA measurements for each pit. The average  $^{55}\text{Mn} / ^{52}\text{Cr}$  RSF for the synthetic calcite is  $0.65 \pm 0.09$  ( $2\sigma$ ).

The synthetic calcite standards had not yet been obtained during the calcite SIMS analyses for Renazzo N1127 and GRO 95577; it was only used as a direct standard for the dolomite in Renazzo N1126. We therefore standardized to San Carlos olivine, and subsequently corrected the data to the calcite RSF. Olivine data measured by EPMA for  $(^{55}\text{Mn} / ^{52}\text{Cr})_{\text{TRUE}}$  were averaged into one value, since the measurements spots were not taken precisely around the individual SIMS pits. The San Carlos olivine RSF did not vary significantly between the two studies: the RSF was  $0.98 \pm 0.15$  and  $0.96 \pm 0.15$  during the calcite and dolomite runs, respectively. The calcite Mn/Cr measurements were corrected for calcite RSF using a bootstrap method, assuming that the difference between the calcite and San Carlos olivine RSF was a constant percentage. We conservatively propagated the uncertainties from the San Carlos olivine and synthetic calcite RSFs to yield a bootstrapped value of  $0.67 \pm 0.14$  ( $2\sigma$ ) to correct the calcite SIMS measurements for Renazzo and GRO 95577 (cf. [supplemental material](#)).

The RSF is dependent on the mineral composition, the instrumental tuning, and the primary beam size (e.g., [Sugiura et al., 2010](#); [McKibbin et al., 2013](#); [Doyle et al., 2016](#)). Therefore, a correction factor used to correct for San Carlos olivine-standardized carbonates on the NanoSIMS will be different than the correction factor needed for San Carlos olivine-standardized carbonates measured at higher currents on the Cameca 1280. It is important to note that there is not a simple “one correction factor fits all” for this issue. The SIMS analysis pits during the two sessions are similar in shape, though the radius of the pits varies by  $\sim 1$ – $2 \mu\text{m}$ . While this change in size may have slightly affected the RSF, the depth of the pits seems to be the dominant source of RSF variation ([Sugiura et al.,](#)

2010; Doyle et al., 2016). In our analyses, the RSF changes by  $\sim 0.1$  from the beginning to end of analysis (cf. [supplemental data Fig. S1](#)). The depth of the SIMS pits in our study appeared uniform across standards and unknowns. Since some analyses for GRO 95577 and Renazzo were divided into multiple data points, there is an additional potential for introducing RSF bias related to depth-dependent variations in the RSF (Sugiura et al., 2010; Doyle et al., 2016). Potential biases are accounted for in the conservative RSF uncertainties.

The RSF for dolomite is poorly constrained. Previous studies of Mn–Cr dating have used the calcite RSF as a proxy for dolomite (e.g., Fujiya et al., 2012, 2013; Jilly et al., 2014). However, this is an active field of study where new estimates for the dolomite RSF are emerging. Recent dolomite synthesis experiments have indicated that the dolomite RSF may be  $\sim 20\%$  greater than that of calcite (Ichimura and Sugiura, 2015). Preliminary studies of ion-implanted carbonates agree, suggesting that the RSF of dolomite is a minimum of  $\sim 15\%$  greater than that of calcite, though the uncertainties are currently too large to determine the value definitively (Steele and McKeegan, 2014). With these issues in mind, we will present the dolomite data using two RSF values: the calcite RSF of  $0.65 \pm 0.09$  determined from our synthetic standard during the dolomite session, and a 20% higher RSF based on this number ( $0.78 \pm 0.11$ ) to represent a hypothetical dolomite RSF with a similar 14% uncertainty. The  $2\sigma$  RSF uncertainties are propagated into the reported uncertainty for the measured  $^{55}\text{Mn}/^{52}\text{Cr}$  ratios.

### 3. RESULTS

#### 3.1. Sample petrography

Renazzo is classified as a moderately altered CR 2 (type 2.4 according to the petrologic scheme of Harju et al., 2014). The host lithology is chondrule-rich, containing numerous metal-rich porphyritic chondrules within a fine-grained matrix. Both matrix and chondrules show evidence of aqueous alteration in the form of secondary minerals. Phyllosilicates comprise the majority of chondrule mesostases, while many chondrule silicates (olivine and pyroxene) remain unaltered. Sub-micron phyllosilicates and clays dominate the fine-grained matrix, often embedded with 3–10  $\mu\text{m}$  Fe–Ni sulfides and magnetite.

Calcite occurs in the matrix in three morphologies: as large, mottled, fine-grained masses that are intergrown with silicates (Fig. 1), as coarse-grained veins that extend up to a few 100  $\mu\text{m}$  in the matrix (Fig. 2a), and as individual coarse grains that occur in the matrix, often near altered chondrules (Fig. 2b). Two coarse-grained calcites from the inter-chondrule matrix in Renazzo N1127 were measured in this work by EPMA and SIMS; the chemical compositions are reported in the [supplementary material \(Table S.2\)](#).

Renazzo is a breccia, and contains numerous dark inclusions. The dark inclusions are chemically and mineralogically very similar to the CR matrix, yet tend to be more hydrated with higher abundances of phyllosilicates, carbon-

ates, sulfides, and magnetite (similar to dark inclusions described in literature, e.g., Weisberg et al., 1993; Kallemeyn et al., 1994). Dolomite is rare in CR chondrites, but numerous grains were found in a dark inclusion from thin section Renazzo N1126 (Fig. 3); framboidal magnetite and Fe-sulfide laths were also pervasive. The crystals are anhedral 5–20  $\mu\text{m}$ -sized grains, found within extensively altered chondrules. We measured the dolomite with EPMA and SIMS. The average molar chemical composition of the dolomite is 49%  $\text{CaCO}_3$ , 41%  $\text{MgCO}_3$ , 1.5%  $\text{MnCO}_3$ , and 9%  $\text{FeCO}_3$  ([supplementary data Table S3](#)).

GRO 95577 is an Antarctic meteorite of petrologic type CR 1, or type 2.0 using the classification scheme of Harju et al. (2014). This sample is the most heavily altered CR chondrite yet documented (e.g., Weisberg and Huber, 2007; Schrader et al., 2011, 2014; Harju et al., 2014), and it is composed almost entirely of secondary minerals. The majority of the thin section studied here is comprised of a single matrix-rich lithology, similar to the dark lithology described in Tyra et al. (2011), though we did not find measurable siderite with the same texture and composition as the grains they described. A similar-looking phase did occur, but was mottled in texture and contained significant ( $\sim 10$  wt%)  $\text{SiO}_2$ , as measured by EDS. All chondrule phenocrysts occur as phyllosilicate pseudomorphs, with chlorite and/or calcite replacing chondrule mesostasis, and magnetite replacing the metal nodules (similar to petrography described in Weisberg and Huber, 2007). The matrix is composed of fine-grained clays and phyllosilicates, with abundant coarse-grained anhedral calcite ( $\sim 5$ – $50$   $\mu\text{m}$  in diameter) embedded throughout. Framboidal magnetite and euhedral to subhedral sulfide platelets co-exist with the calcite in the matrix, and are often intergrown (Fig. 4). All calcite grains measured here come from within the matrix. The chemical compositions of the GRO 95577 calcite grains are reported in the [supplementary material \(Table S2\)](#).

#### 3.2. $^{53}\text{Mn}$ – $^{53}\text{Cr}$ measurements of matrix calcite

Two calcite grains were measured for  $^{53}\text{Mn}$ – $^{53}\text{Cr}$  isotope systematics in Renazzo N1127. Both grains are in the host lithology matrix (rather than in a dark inclusion or foreign clast). The calcite grains range from  $\sim 20$   $\mu\text{m}$  in the shortest dimension, to  $\sim 100$   $\mu\text{m}$  at the longest (Fig. 5a and b). One grain occurs as an isolated matrix grain (Fig. 5a), and the other is in the matrix adjacent to a chondrule (Fig. 5b). Additional calcite grains were targeted, but the  $^{55}\text{Mn}^+$  and  $^{52}\text{Cr}^+$  count rates were far too low to be measured due to high purity of the mineral. The fractionation- and RSF-corrected isotope data are presented in Table 2. The maximum  $\delta^{53}\text{Cr}^*$  value is  $\sim 230$ , and the maximum  $^{55}\text{Mn}/^{52}\text{Cr}$  is  $\sim 7300$ .

Five calcite grains in GRO 95577 were found with high enough count rates to be measured for Mn and Cr. The measured calcite grains in GRO 95577,69 were each about 20  $\mu\text{m}$  in diameter, all existing within the altered matrix (Fig. 5c and d). The maximum  $\delta^{53}\text{Cr}^*$  value is  $\sim 1000$  and the RSF-corrected maximum  $^{55}\text{Mn}/^{52}\text{Cr}$  ratio is  $\sim 120,000$  (Table 2). The two data points with the highest  $^{55}\text{Mn}/^{52}\text{Cr}$

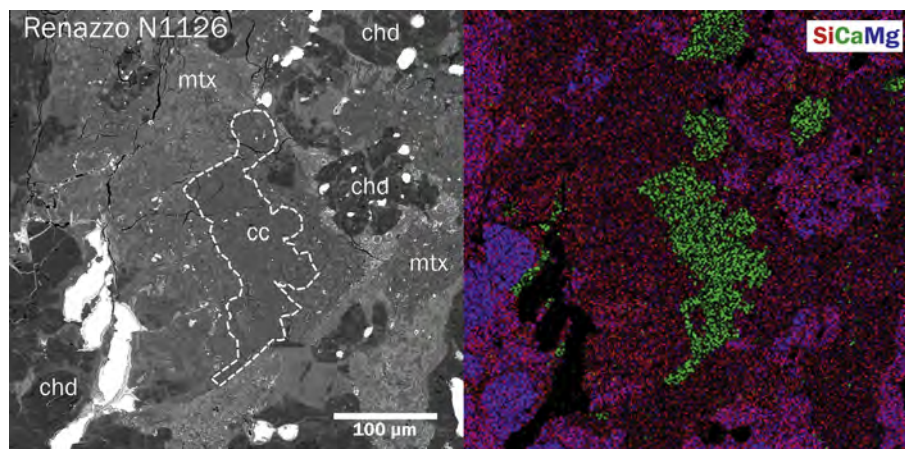


Fig. 1. Backscattered electron (BSE) image (left) of fine-grained Ca-carbonate material in the phyllosilicate-rich matrix of Renazzo N1126 (outlined by the dashed line). The carbonate is intergrown with phyllosilicates and sulfides, making it unsuitable for  $^{53}\text{Mn}$ - $^{53}\text{Cr}$  measurements. The false color EDX map (right) depicts Si in red, Ca in green, and Mg in blue. chd = chondrule, cc = calcite, mtx = matrix.

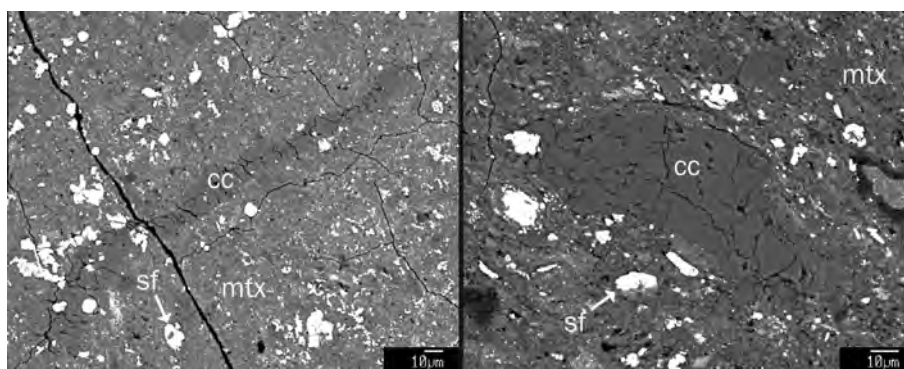


Fig. 2. BSE images of calcite in the Renazzo N1127 matrix. The image on the left shows a calcite vein extending  $>100\ \mu\text{m}$  across the matrix. On the right is a coarse-grained calcite from the interchondrule matrix. The bright phases in both images are Fe-sulfides. cc = calcite, mtx = matrix, sf = sulfide.

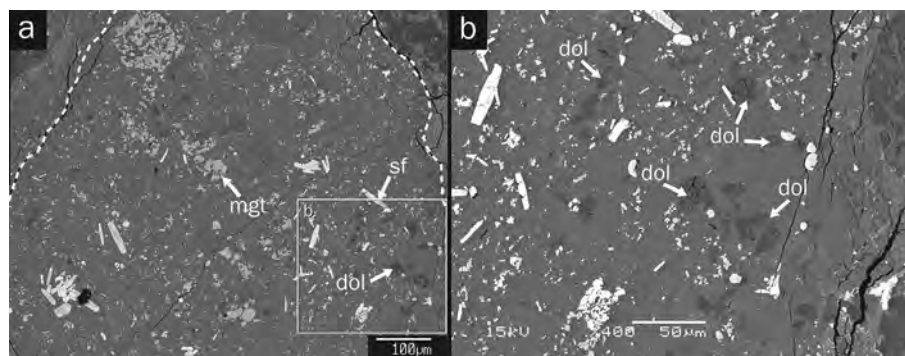


Fig. 3. (a) BSE image of a dark inclusion in Renazzo N1126. The dashed lines outline the borders of the dark inclusion clast. This lithology consists of phyllosilicate groundmass, and contains abundant magnetite framboids, sulfide laths, and dolomite crystals. (b) Larger image of the area in the square box from 3a to show the dolomite crystals. dol = dolomite, mgt = magnetite, sf = sulfide.

ratios correspond to a carbonate grain enriched in Mn relative to the other GRO 95577 calcites measured here by EPMA (see [supplementary data](#)).

The  $\delta^{53}\text{Cr}^*$  values from calcite grains in Renazzo N1127 and GRO 95577 are correlated with the  $^{55}\text{Mn}/^{52}\text{Cr}$  ratios. On a plot of  $^{53}\text{Cr}/^{52}\text{Cr}$  versus  $^{55}\text{Mn}/^{52}\text{Cr}$  (Fig. 6), the

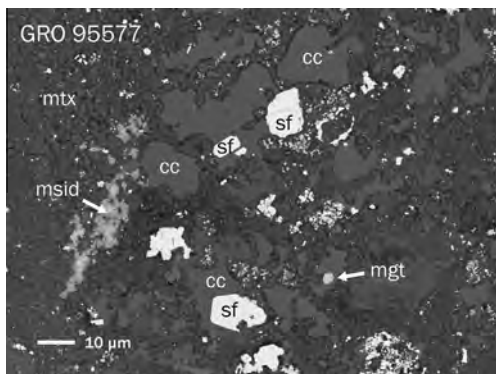


Fig. 4. BSE image of matrix phases in GRO 95577. The matrix consists of a fine-grained phyllosilicate groundmass embedded with secondary calcite, sulfide, and magnetite grains. cc = calcite, mgt = magnetite, msid = mottled siderite, mtx = matrix, sf = sulfide.

correlation trend for Renazzo calcites has a slope of  $(3.6 \pm 2.7) \times 10^{-6}$ , with  $\chi_{\text{red}}^2 = 0.76$ . The correlation trend for the GRO 95577 calcites has a slope of  $(7.9 \pm 2.8) \times 10^{-7}$ , with  $\chi_{\text{red}}^2 = 0.60$ . The slopes of both trends are resolved from zero. The  $\chi_{\text{red}}^2$  values suggest that the scatter in the data can be explained by stochastic statistical fluctuation, and that the errors are conservatively estimated. The large uncertainty in the slope is dominated by the uncertainty in  $\delta^{53}\text{Cr}^*$  due to low count rates. For GRO 95577, data points cc #2 and cc #3a have sufficiently correlated errors to be visible in the plot, as shown in the inset image of Fig. 6.

### 3.3. $^{53}\text{Mn}$ – $^{53}\text{Cr}$ measurements of dolomite from a dark inclusion

We measured seven dolomite grains in a Renazzo N1126 dark inclusion (Fig. 5e, f). Similar to the calcite analyses, additional dolomite grains were targeted for measurement,

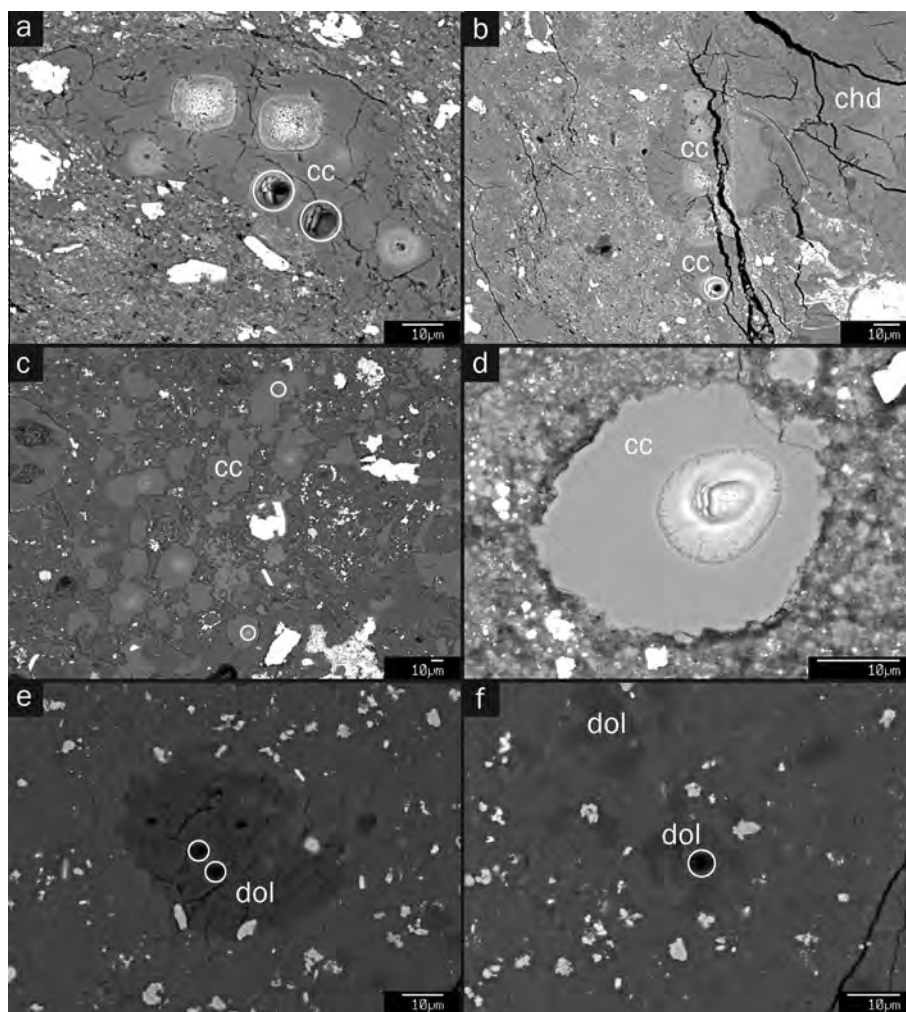


Fig. 5. BSE image of typical carbonates measured for  $^{53}\text{Mn}$ – $^{53}\text{Cr}$  in this study.  $^{53}\text{Mn}$ – $^{53}\text{Cr}$  pits are circled in white. (a, b) Calcite grains cc #4 and #2 (Table 2) in Renazzo N1127. O isotope pits and electron beam damage are also visible on both grains. (c) Calcite grains in the matrix of GRO 95577, cc #3 (top circle), and cc #4 (bottom). Some O isotope pits are visible on other grains. (d) Enlarged image of a calcite grain (cc #1) in GRO 95577 measured for  $^{53}\text{Mn}$ – $^{53}\text{Cr}$ . (e, f) Dolomite grains from a dark inclusion in Renazzo N1126. Analyses dol #1a and #1b (Table 3) are shown in (e), and dol #2 is shown in (f). chd = chondrule, cc = calcite, dol = dolomite.

Table 2  
Mn–Cr isotopes in matrix calcite from CR chondrites. All errors are  $2\sigma$ .

Sample	Grain	$^{53}\text{Cr}/^{52}\text{Cr}$	$\delta^{53}\text{Cr}^*$	$^{55}\text{Mn}/^{52}\text{Cr}^a$	$^{52}\text{Cr}_{\text{tot}}^b$	$^{55}\text{Mn}^c$	$\rho(x,y)^d$			
Renazzo N1127	cc #2	0.1123	$\pm 0.0067$	$-10$	$\pm 59$	37	$\pm 8$	45872	554	0.2
	cc #4a	0.1199	$\pm 0.0066$	56	$\pm 58$	652	$\pm 134$	11132	1934	0.1
	cc #4b	0.1123	$\pm 0.0077$	$-10$	$\pm 68$	452	$\pm 94$	4869	1918	$-0.2$
	cc #4c	0.1190	$\pm 0.0098$	49	$\pm 87$	1985	$\pm 410$	7293	4708	0.1
	cc #4d	0.1391	$\pm 0.0212$	226	$\pm 186$	7330	$\pm 1534$	2387	5021	0.2
GRO 95577	cc #1	0.1288	$\pm 0.0243$	135	$\pm 214$	4877	$\pm 1038$	1297	2335	0.1
	cc #2	0.1356	$\pm 0.0363$	195	$\pm 320$	9893	$\pm 2131$	946	3067	0.5
	cc #3a	0.1507	$\pm 0.0201$	328	$\pm 178$	52203	$\pm 10933$	2303	65854	0.4
	cc #3b	0.2321	$\pm 0.0446$	1045	$\pm 393$	123804	$\pm 26781$	862	70068	0.3
	cc #4	0.1174	$\pm 0.0116$	35	$\pm 102$	2334	$\pm 485$	3632	2786	0.0
	cc #12	0.1240	$\pm 0.0243$	93	$\pm 214$	2241	$\pm 470$	2125	1564	0.2

<sup>a</sup> Uncertainty in the RSF is included in the  $^{55}\text{Mn}/^{52}\text{Cr}$  ratio error.

<sup>b</sup> Sum of all counts per measurement.

<sup>c</sup> Total counts per measurement cycle.

<sup>d</sup> Linear correlation coefficient between  $^{53}\text{Cr}/^{52}\text{Cr}$  and  $^{55}\text{Mn}/^{52}\text{Cr}$  for each run.

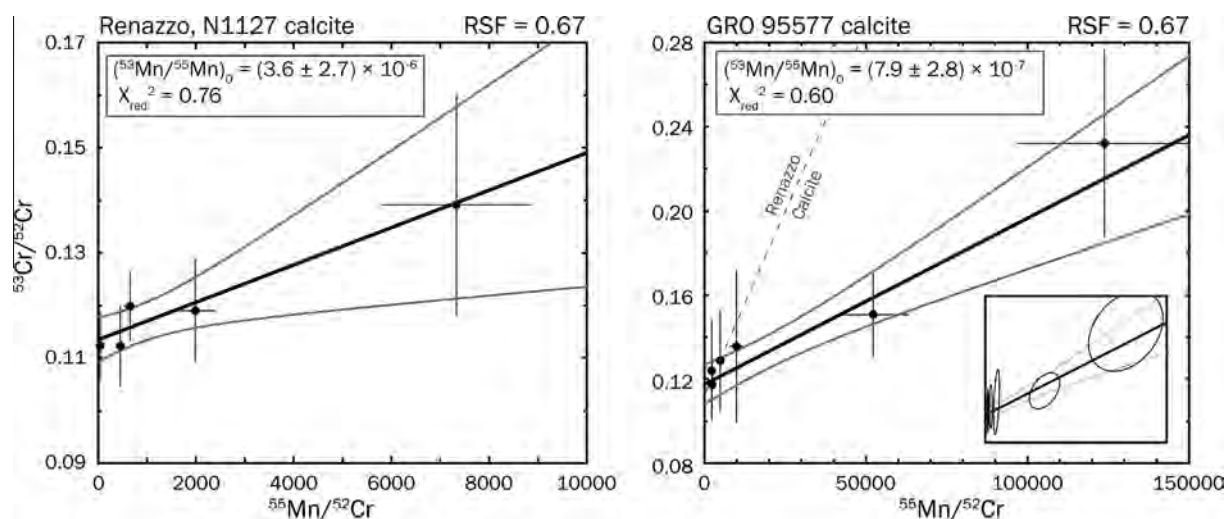


Fig. 6.  $^{53}\text{Cr}/^{52}\text{Cr}$  versus  $^{55}\text{Mn}/^{52}\text{Cr}$  in calcites from Renazzo N1127 and GRO 95577. Solid black lines are error-weighted least-squares regressions through the data (model 1 fit in Isoplot). The slope of the regression gives the initial  $(^{53}\text{Mn}/^{55}\text{Mn})_0$  ratio. Error crosses represent  $2\sigma$  uncertainties. The error envelope for the regression is shown with grey lines. For GRO 95577, some data had significantly correlated errors, as depicted as error ellipses in the inset box.

but were too pure to yield adequate count rates for Mn and Cr isotopes. The maximum dolomite  $\delta^{53}\text{Cr}^*$  value is  $\sim 290$ , and the maximum  $^{55}\text{Mn}/^{52}\text{Cr}$  value is  $\sim 9300$  for RSF = 0.65, or  $\sim 7800$  for RSF = 0.78 (Table 3).

The  $\delta^{53}\text{Cr}^*$  values correlate with the  $^{55}\text{Mn}/^{52}\text{Cr}$  ratio on a plot of  $^{53}\text{Cr}/^{52}\text{Cr}$  versus  $^{55}\text{Mn}/^{52}\text{Cr}$  (Fig. 7). For the RSF of 0.65, the slope of the dolomite correlation is  $(3.1 \pm 1.4) \times 10^{-6}$ , with  $\chi^2_{\text{red}} = 0.94$ . Applying the inferred dolomite RSF of 0.78, the slope increases to  $(3.7 \pm 1.7) \times 10^{-6}$ , with  $\chi^2_{\text{red}} = 0.94$ . The  $\chi^2_{\text{red}}$  values indicate that the fluctuations in the data are dominated by statistical variation. The slope of the correlation trend depends on the RSF value used (Fig. 8). As the RSF decreases, the slope of the array on the Mn–Cr diagram also decreases. The calcite RSF may range from 0.56 to 0.74 (within uncertainty limits), and although the dolomite RSF has been estimated to be  $\sim 20\%$  higher, this value is very imprecise. Until a con-

crete dolomite RSF has been determined, all Mn–Cr data on dolomite must be interpreted cautiously with this issue in mind.

#### 4. DISCUSSION

We found five points from Renazzo (four dolomite, one calcite) and two from GRO 95577 that have well resolved  $\delta^{53}\text{Cr}^*$ , while a large number of carbonates have  $^{53}\text{Cr}/^{52}\text{Cr}$  compositions that are close to normal with low  $^{55}\text{Mn}/^{52}\text{Cr}$  ratios. In this section, we discuss the petrographic context of the measured carbonates, and make the case that the carbonates were formed during aqueous alteration on the CR chondrite parent body. The validity of the isochron diagrams and absolute ages are discussed. We investigate possible formation processes for the carbonates, with a particular focus on different heating mechanisms that drive

Table 3

Mn–Cr isotopes in dolomite from Renazzo N1126. All errors are  $2\sigma$ . Data for RSF values of 0.65 and 0.78 are given.

Grain	$^{53}\text{Cr}/^{52}\text{Cr}$	$\delta^{53}\text{Cr}$	$^{55}\text{Mn}/^{52}\text{Cr}$ (RSF = 0.65) <sup>a</sup>	$^{55}\text{Mn}/^{52}\text{Cr}$ (RSF = 0.78) <sup>a</sup>	$^{52}\text{Cr}_{\text{tot}}$ <sup>b</sup>	$^{55}\text{Mn}^c$	$\rho(x,y)^d$
dol #1a	$0.1177 \pm 0.0050$	$37 \pm 44$	$918 \pm 129$	$765 \pm 107$	21800	5188	0.0
dol #1b	$0.1243 \pm 0.0112$	$95 \pm 99$	$3128 \pm 446$	$2606 \pm 371$	4559	4019	0.1
dol #2	$0.1321 \pm 0.0132$	$164 \pm 117$	$6552 \pm 940$	$5460 \pm 781$	3491	5686	0.3
dol #4a	$0.1232 \pm 0.0117$	$86 \pm 103$	$2265 \pm 324$	$1888 \pm 269$	4129	4444	0.2
dol #4b	$0.1206 \pm 0.0094$	$63 \pm 83$	$1435 \pm 203$	$1195 \pm 169$	6266	4124	0.3
dol #5	$0.1214 \pm 0.0122$	$70 \pm 107$	$5503 \pm 788$	$4586 \pm 655$	3746	7626	0.3
dol #8	$0.1345 \pm 0.0279$	$186 \pm 246$	$5750 \pm 899$	$4792 \pm 747$	799	8928	0.3
dol #11a	$0.1406 \pm 0.0227$	$239 \pm 200$	$7050 \pm 1059$	$5875 \pm 881$	1272	5651	0.2
dol #11b	$0.1460 \pm 0.0285$	$286 \pm 251$	$9336 \pm 1452$	$7780 \pm 1208$	843	5168	0.3
dol #12	$0.1453 \pm 0.0130$	$281 \pm 115$	$5864 \pm 838$	$4886 \pm 696$	4020	10085	0.3

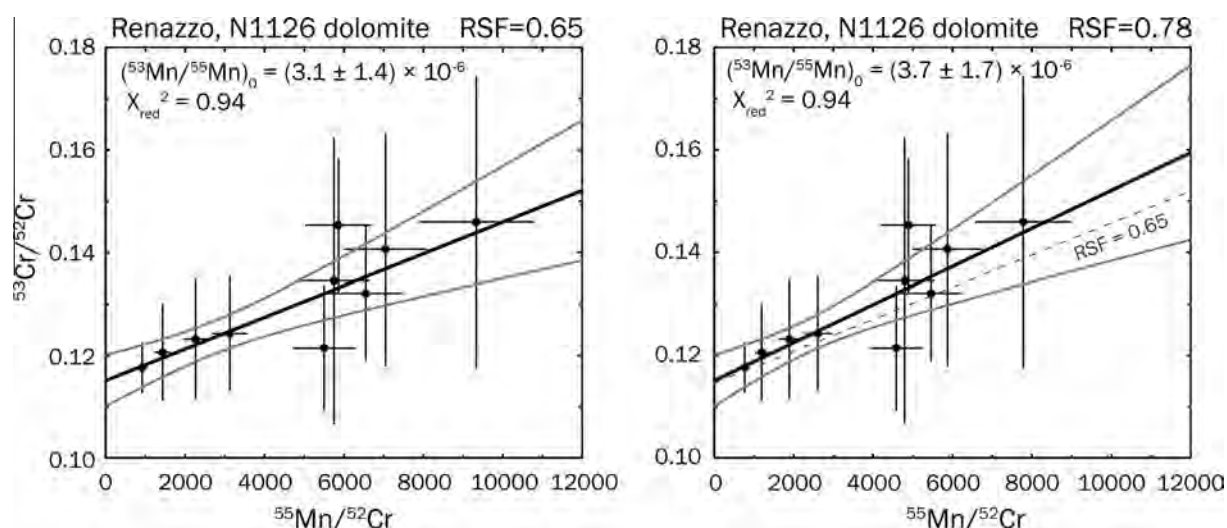
<sup>a</sup> Uncertainty in the RSF is included in the  $^{55}\text{Mn}/^{52}\text{Cr}$  ratio error.<sup>b</sup> Sum of all counts per measurement.<sup>c</sup> Total counts per measurement cycle.<sup>d</sup> Linear correlation coefficient between  $^{53}\text{Cr}/^{52}\text{Cr}$  and  $^{55}\text{Mn}/^{52}\text{Cr}$  for each run.

Fig. 7.  $^{53}\text{Cr}/^{52}\text{Cr}$  versus  $^{55}\text{Mn}/^{52}\text{Cr}$  for dolomite from a Renazzo N1126 dark inclusion. The two panels represent the same measurements corrected to different RSF values: the calcite RSF of 0.65 of the left, and an inferred dolomite RSF of 0.78 on the right. Data are fitted with a weighted least-squares regression (model 1 fit in Isoplot) shown as a solid black line, with error envelope as gray lines. The dashed line in the right panel is the slope of the RSF = 0.65 regression for comparison. The regression slopes are expressed as the initial ( $^{53}\text{Mn}/^{55}\text{Mn}$ )<sub>0</sub> ratio. Error crosses represent  $2\sigma$  uncertainty, as described in text.

the parent body alteration process. Lastly, we compare our results with the literature data for other chondrite groups, and investigate potential inconsistencies between  $^{53}\text{Mn}$ – $^{53}\text{Cr}$  data and data from other radiometric dating systems in CR chondrites.

#### 4.1. Support for parent-body aqueous alteration

The mineral morphologies and petrographic textures observed in CR chondrites are consistent with carbonate formation on the CR parent body, rather than in a nebular environment. Several lines of petrographic evidence support this model: (1) Pre-terrestrial calcite veins (Fig. 2) in the interchondrule matrix indicate *in situ* alteration, as they are formed by small-scale fluid flow (e.g., Endreß and Bischoff, 1996). (2) Partially leached chondrules show evidence of elements having been transported from altered

glassy mesostasis and deposited in the surrounding matrix as a secondary mineral (e.g., Fig. 9). This style of alteration is common in CR chondrites, indicating interaction of water between the two lithologies (e.g., Burger and Brearley, 2004; Brearley, 2006). (3) Framboidal magnetite and sulfide morphologies are ubiquitous in CR chondrites and indicative of formation from a fluid-rich environment, not possible in the nebula (e.g., Ikeda and Prinz, 1993; Sawłowicz, 2000; Astafieva et al., 2004).

An earlier nebular or pre-accretionary history of hydration cannot be ruled out entirely if overprinted by the subsequent parent body aqueous alteration. It has been argued that phyllosilicate rims and clasts may have formed by the reaction of primary silicates with nebular gas (Ikeda and Prinz, 1993; Ichikawa and Ikeda, 1995) to explain sharp boundaries between chondrule and matrix phyllosilicates that have different chemical compositions. However, similar

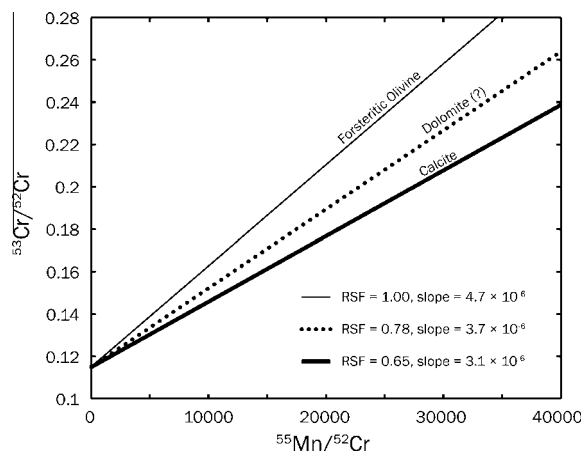


Fig. 8. The effect of RSF on  $^{53}\text{Cr}/^{52}\text{Cr}$  versus  $^{55}\text{Mn}/^{52}\text{Cr}$  correlations. The trend depicted here is from the dolomite measured in Renazzo N1126. The various lines show what the inferred slope value would be for different RSF values used here and in literature.

sharp boundaries seen in the heavily altered GRO 95577 suggest that water-rich, parent-body alteration in CR chondrites can also preserve the textural integrity of the primary components (Weisberg and Huber, 2007).

The O isotopic compositions of CR carbonates further support the parent body alteration model. The carbonate O isotopic compositions from five different CR chondrites plot along a mass-independent fractionation array of slope  $\sim 0.63$  on a standard O three-isotope diagram. (Jilly-Rehak et al., 2015). This array has been interpreted as a progressive alteration trend, where the carbonates formed from a constantly evolving fluid. This O-isotope-evolution model is consistent with the closed-system, phyllosilicate-dominated parent body alteration models invoked for CM chondrite alteration trends (e.g., Clayton and Mayeda, 1984, 1999; Benedix et al., 2003; Bland et al., 2009). Furthermore, the O compositions of calcite and magnetite in GRO 95577 fall on a single mass-dependent fractionation line, indicating that they were formed locally from the same fluid. The fractionation between magnetite and calcite constrains the alteration temperatures to be around  $\sim 10\text{--}60\text{ }^\circ\text{C}$  (Jilly-Rehak et al., 2015). Such conditions would be difficult to maintain in a turbulent and disruptive pre-accretionary hydration environment (e.g., Brearley, 2006), but are consistent with parent-body alteration (e.g., Clayton and Mayeda, 1977, 1999).

Lastly, carbonates can potentially form during terrestrial weathering. Previous studies have shown that terrestrial calcite veins can form even in falls (e.g., Abreu and Brearley, 2005; Bland et al., 2006). The mineral textures, non-terrestrial O isotopic compositions (e.g., Abreu and Brearley, 2005; Jilly and Huss, 2012; Jilly-Rehak et al., 2015), and excesses of radiogenic  $^{53}\text{Cr}$  in the carbonates presented here are inconsistent with an origin from terrestrial weathering.

#### 4.2. Validity of isochron diagrams

In principle, the correlation between  $\delta^{53}\text{Cr}^*$  and the  $^{55}\text{Mn}/^{52}\text{Cr}$  ratio can either reflect the radioactive decay of

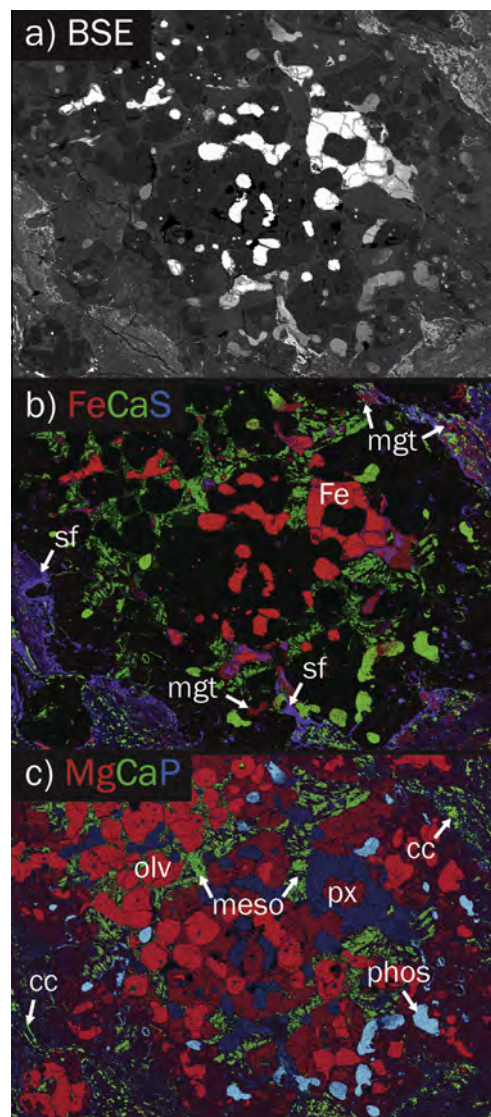


Fig. 9. Images of a partially altered chondrule in Renazzo N1127. The first X-ray map depicts Fe, Ca, and S in red, blue, and green false color. The second map depicts Si, Ca, and phosphorous. These false-colored maps show that the exterior of the chondrule has been partially altered, where Ca, Al, Fe, and Si have all been mobilized. Ca has precipitated in the matrix as calcite, and within chondrule nodules as hydroxyapatite. Fe has been mobilized from the metal nodules into the matrix as magnetite. S is mobilized from the matrix into the chondrule, replacing Fe-metal with Fe-sulfides. cc = calcite, Fe = Fe-metal, meso = feldspathic mesostasis, mgt = magnetite, olv = primary olivine, phos = phosphate (likely hydroxyapatite), px = primary pyroxene, sf = sulfide.

$^{53}\text{Mn}$  after mineral formation, or it can represent a mixing line without time significance. Such a mixing line can result from mixing variable amounts of normal Cr with a component enriched in  $^{53}\text{Cr}$  (Hoppe et al., 2007; Fujiya et al., 2013). This is because both  $^{53}\text{Cr}/^{52}\text{Cr}$  and  $1/^{52}\text{Cr}$  would increase with decreasing  $^{52}\text{Cr}$  (from the normal component), if contaminated with a constant  $^{53}\text{Cr}$ -enriched component. If the excess  $^{53}\text{Cr}$  is instead due to the decay of  $^{53}\text{Mn}$ , and the Mn abundance is constant among a set of

samples, a linear array can still result if the Cr abundance varies across the set of samples. Such an array is indistinguishable from the mixing line discussed above without additional information. On the other hand, if  $^{53}\text{Mn}$  was alive when a sample formed and the Mn abundance varied independently from Cr, the amount of excess  $^{53}\text{Cr}$  will correlate with the  $^{55}\text{Mn}/^{52}\text{Cr}$  ratio, but it will not correlate with  $1/^{52}\text{Cr}$ . The  $^{55}\text{Mn}$  abundances in our data vary by at least a factor of two for Renazzo calcite and dolomite (Tables 2 and 3), and the  $^{55}\text{Mn}$  in GRO 95577 is variable by an order of magnitude (Table 2). The correlations between  $\delta^{53}\text{Cr}^*$  and  $^{55}\text{Mn}/^{52}\text{Cr}$  for our data are stronger than the correlations between  $\delta^{53}\text{Cr}^*$  and  $1/^{52}\text{Cr}^+$  for all

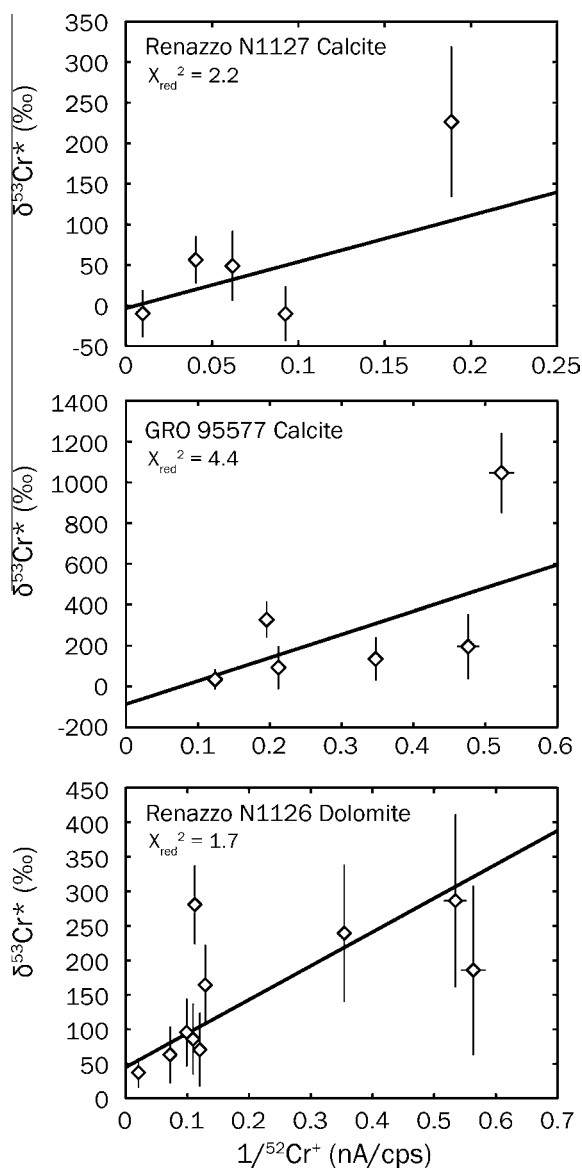


Fig. 10. Graphs of  $\delta^{53}\text{Cr}^*$  versus  $1/^{52}\text{Cr}^+$ . The  $1/^{52}\text{Cr}^+$  values are given as the inverse of the counts per second normalized to beam current. The variability in  $1/^{52}\text{Cr}^+$  and higher values of  $\chi^2_{\text{red}}$  for the data on these diagrams support the interpretation of the correlations in Figs. 6 and 7 as isochrons. Errors are  $1\sigma$ .

of our data (cf. Figs. 6, 7 and 10), showing that the arrays in Figs. 6 and 7 result from the decay of  $^{53}\text{Mn}$ . Therefore, the variable Mn concentrations likely represent zoning or varied Mn incorporation during carbonate precipitation, rather than contamination from a Cr-bearing phase. We interpret the excess of  $^{53}\text{Cr}$  in the carbonates as being the decay product of live  $^{53}\text{Mn}$ , where the slope of the correlation represents the initial ratio of  $(^{53}\text{Mn}/^{55}\text{Mn})_0$  incorporated into the carbonate grains when formed by aqueous alteration.

The isochron validity depends on the assumption that all measured grains formed during a single alteration event. This assumption is reasonable for our measurements, as the grains considered for each isochron exist in the same lithology. We only measured coarse-grained calcites in the inter-chondrule matrix in Renazzo and GRO 95577, and the Renazzo dolomites were measured in a single dark inclusion. Support for a single alteration event comes from O isotopes. Clustered O isotopic compositions of carbonate grains in a single lithology (Jilly-Rehak et al., 2015) suggest that the fluid did not evolve significantly during the formation of the carbonates. If zonation in the carbonates are the result of discrete alteration events, the events must have occurred under uniform O-isotopic fluid conditions, and within the temporal resolution and uncertainty of the  $^{53}\text{Mn}$ - $^{53}\text{Cr}$  chronometer.

There are two ways to interpret the isochron for GRO 95577. The slope of the isochron in Fig. 6 is controlled by two points from a single grain with high Mn/Cr, while the other four points near the origin have an apparently steeper slope of  $(2.5 \pm 4.6) \times 10^{-6}$  if considered separately (Fig. 11). The steep slope of the inner array could imply that there were two stages of aqueous alteration in GRO 95577. While this hypothesis is intriguing, the uncertainties are too large and the slope is unresolved from zero; it will therefore not be seriously considered. The apparent slope is likely an artifact from uncertainty. Furthermore, there is no textural (Fig. 5c) or O-isotopic evidence (Jilly-Rehak et al., 2015) that the grains should represent distinct events. Therefore, the GRO 95577 isochron is best interpreted as dating a single alteration event.

### 4.3. D'Orbigny as a suitable $^{53}\text{Mn}$ - $^{53}\text{Cr}$ absolute age anchor

To obtain accurate absolute ages, the measured  $(^{53}\text{Mn}/^{55}\text{Mn})_0$  must be anchored to another object that has been dated using multiple short-lived and long-lived radiometric systems. The initial  $^{53}\text{Mn}/^{55}\text{Mn}$  of the Solar System ( $(^{53}\text{Mn}/^{55}\text{Mn})_{\text{SS}}$ ) is poorly constrained, with estimates ranging from  $(6.3 \pm 0.7) \times 10^{-6}$  to  $(9.1 \pm 1.7) \times 10^{-6}$  (Trinquier et al., 2008; Nyquist et al., 2009). The initial solar system abundance remains uncertain due to the relative lack of minerals in CAIs with high Mn/Cr ratios, to disturbances in the Mn-Cr system in such minerals by secondary processing, to intrinsic isotopic anomalies in Cr in CAIs, and to difficulties in establishing  $^{53}\text{Mn}$  homogeneity in the solar nebula (e.g., Birk and Allègre, 1984; Lugmair and Shukolyukov, 1998; Birck et al., 1999; Nyquist et al., 2001, 2009; Papanastassiou et al., 2005). Angrites – a class of igneous, achondritic meteorites – are

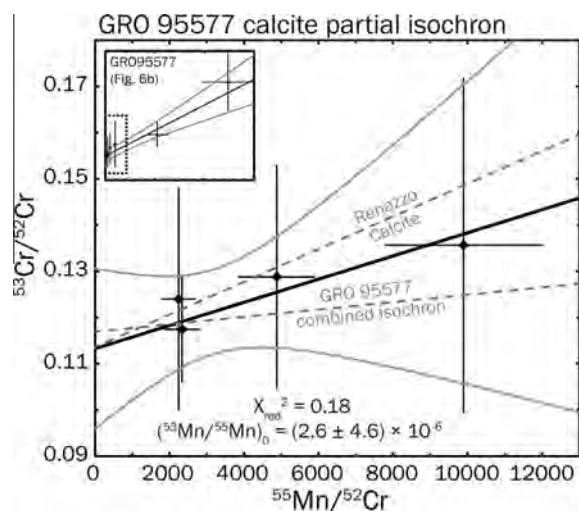


Fig. 11. Isochron diagram depicting the inner four data points from the GRO 95577 calcite diagram (inset, Fig. 6b). The regression has a poor fit and is not resolved from zero. The isochron slopes for Renazzo and GRO 95577 from Fig. 6 are depicted as grey dashed lines for comparison.

commonly used for anchoring of  $^{53}\text{Mn}$ – $^{53}\text{Cr}$  analyses, but there are disagreements within the scientific community regarding which angrite is the best time-anchor (for detailed discussions on this issue, see Schiller et al., 2010; Brennecka and Wadhwa, 2012; Keil, 2012; Kleine et al., 2012; Kruijjer et al., 2014; McKibbin et al., 2015).

We anchored our measurements to the D’Orbigny angrite. D’Orbigny is a volcanic “quenched” angrite that has been thoroughly studied with a variety of radiometric systems and makes a suitable time-anchor, as the  $^{26}\text{Al}$ – $^{26}\text{Mg}$ ,  $^{182}\text{Hf}$ – $^{182}\text{W}$ , and Pb–Pb isochron ages are concordant, assuming that the live radionuclides were homogeneously distributed in the CAI and angrite forming regions of the solar nebula (e.g., Mittlefehldt et al., 2002; Glavin et al., 2004; Spivak-Birndorf et al., 2009; Schiller et al., 2010; Keil, 2012; Kleine et al., 2012; Kruijjer et al., 2014; McKibbin et al., 2015). D’Orbigny is one of the largest, best dated, and oldest angrites that crystallized while  $^{26}\text{Al}$  was still alive, providing ages for silicates using the  $^{26}\text{Al}$ – $^{26}\text{Mg}$  system. The  $^{26}\text{Al}$ – $^{26}\text{Mg}$  isochrons of D’Orbigny and the co-magmatic Sahara 99555 angrite (Spivak-Birndorf et al., 2009; Schiller et al., 2010) yield ages that are concordant with  $^{182}\text{Hf}$ – $^{182}\text{W}$  ages, based on the revised initial solar system abundance for  $^{182}\text{Hf}/^{180}\text{Hf}$  (Kleine et al., 2012; Kruijjer et al., 2014), and a canonical initial solar system abundance of  $^{26}\text{Al}/^{27}\text{Al}$  of  $5.23 \times 10^{-5}$  (Jacobsen et al., 2008).

The issue becomes more complicated when comparing Pb–Pb chronometry of angrites with that of CAIs, to determine when in solar system history the angrites formed. The initial solar system abundances of  $^{26}\text{Al}$  and  $^{182}\text{Hf}$  are taken to represent the abundances present at the time of CAI formation, cosmochemically considered to be “time zero”. At present, there are few U-isotope corrected Pb–Pb ages of CAIs to connect the short-lived radionuclides to the abso-

lute time scale. Estimates of the absolute Pb–Pb ages range from  $\sim 4567$  to  $\sim 4568$  Ma (Amelin et al., 2010; Bouvier and Wadhwa, 2010; Bouvier et al., 2011; Connelly et al., 2012), and the source of this discrepancy is currently unknown. If the Pb–Pb angrite ages are measured relative to the Pb–Pb CAI age of  $4567.30 \pm 0.16$  (Connelly et al., 2012), then they are inconsistent with the  $^{26}\text{Al}$ – $^{26}\text{Mg}$  and  $^{182}\text{Hf}$ – $^{182}\text{W}$  ages. Both the D’Orbigny and Sahara 99555 Pb–Pb ages are in better agreement with  $^{26}\text{Al}$ – $^{26}\text{Mg}$  and  $^{182}\text{Hf}$ – $^{182}\text{W}$  when taken relative to the Pb–Pb CAI age of  $4567.94 \pm 0.31$  (Bouvier et al., 2011) as discussed in Kruijjer et al. (2014). Some have argued that discrepancies between the short-lived and long-lived ages of angrites and CAIs may be due to factors such as heterogeneity of  $^{26}\text{Al}$  in the early solar system (e.g., Larsen et al., 2011), Mg-isotope diffusion in feldspars from angrites (Schiller et al., 2010; Kleine et al., 2012), or anomalous initial ratios for short-lived radionuclide systems (Kruijjer et al., 2014). While this controversy remains a topic of debate, will use the Bouvier et al. (2011) Pb–Pb CAI age for the purpose of this paper due to consistency with the short-lived systems.

Assuming homogeneous distribution of  $^{53}\text{Mn}$  in the chondrite-forming region of the early Solar System, we obtain the absolute ages by comparing the relative initial ( $^{53}\text{Mn}/^{55}\text{Mn}$ )<sub>0</sub> ratios of the CR chondrite carbonates to that of D’Orbigny. The  $^{53}\text{Mn}$ – $^{53}\text{Cr}$  isochron slopes determined here are anchored to the D’Orbigny U-isotope-corrected Pb–Pb age of  $4563.37 \pm 0.25$  Ma (Amelin, 2008; Brennecka and Wadhwa, 2012). We use the revised D’Orbigny initial ( $^{53}\text{Mn}/^{55}\text{Mn}$ )<sub>0</sub> ratio of  $(3.54 \pm 0.18) \times 10^{-6}$  (McKibbin et al., 2015) instead of  $(3.24 \pm 0.04) \times 10^{-6}$  from Glavin et al. (2004). McKibbin et al. (2015) measured Mn–Cr systematics using SIMS, where the isochron slope is dominated by the mineral kirschsteinite (CaFe (SiO<sub>4</sub>)). This mineral is argued to provide greater resistance to Cr cation diffusion (McKibbin et al., 2015), as compared with the Ca-poor olivine that dominated the isochrons from the TIMS measurements of Glavin et al. (2004). The diffusion of Cr is potentially reliant on the silica activity and the diffusion of Al, which can be very slow relative to other cations (Spandler and O’Neill, 2010; Zhukova et al., 2014a,b; McKibbin et al., 2015).

#### 4.4. Absolute ages and implications for aqueous alteration on the CR parent body

The isochron slopes yield ages of  $4563.4^{+2.8}/_{-7.4}$  Ma for the Renazzo N1127 calcite, and  $4555.4^{+1.4}/_{-2.1}$  Ma for GRO 95577 calcite with the D’Orbigny anchor. These correspond to relative ages of  $4.6^{+7.4}/_{-2.8}$  Myr after CAI formation for Renazzo calcites, and  $12.6^{+2.1}/_{-1.4}$  Myr after CAI formation for GRO 95577 calcites (using the CAI formation age of  $4567.94 \pm 0.31$  Ma from Bouvier et al., 2011). For the Renazzo dolomites, we obtain absolute ages of  $4562.6^{+1.7}/_{-3.0}$  Ma (RSF = 0.65) or  $4563.6^{+1.7}/_{-3.0}$  Ma (RSF = 0.78). This yields ages of  $5.3^{+3.0}/_{-1.7}$  or  $4.3^{+3.0}/_{-1.7}$  Myr after CAI formation for the RSF values of 0.65 and 0.78, respectively. The errors are dominated by the  $2\sigma$  statistical uncertainty in the measurement, but also

include the uncertainty in the RSF and the uncertainty in the Mn–Cr age of D'Orbigny.

#### 4.4.1. Early onset of alteration on the CR parent body

The Renazzo  $^{53}\text{Mn}$ – $^{53}\text{Cr}$  carbonate ages ( $\sim 4$ – $5$  Myr after CAI formation) provide evidence for the early onset of aqueous alteration on the CR parent body. Differences in the ages of calcite and dolomite cannot be resolved with our data. While the dark inclusions in Renazzo do not appear to have been altered *in situ* in the breccia (Fig. 3a), we cannot distinguish the timing of alteration of the Renazzo matrix lithology as compared with dark inclusions.

Models of asteroidal accretion suggest that the carbonaceous chondrite parent bodies accreted near the snow line, at a distance ( $\sim 2$ – $5$  AU) where the temperature was cold enough for water to condense into icy grains (e.g., Jewitt et al., 2007). The hydrated lithologies observed here (c.f. Section 3.1.) indicate that water was present on the CR parent body, likely accreted as ice along with the anhydrous precursor components such as matrix, chondrules, etc. (Grimm and McSween, 1989; Brearley, 2006). Aqueous alteration does not effectively occur between rock and ice; rather, water must exist as a fluid for alteration to proceed. Both the pressure and the temperature must be above the triple point of 611 Pa and 273.16 K for liquid water to be stable on the parent body. Very small bodies ( $r < 2$  km) can never sustain the triple-point pressure, and any heating of such bodies would cause sublimation of water-ice (Jewitt et al., 2007). Therefore, the aqueously altered chondritic parent bodies must have had radii  $\geq 2$  km (for average density  $\rho = 10^3$  kg/m $^3$ ) to maintain liquid water in the interior.

Accretional heating (from the release of gravitational energy upon formation) is an important heat source for large bodies, but is insufficient to melt ice on the smaller undifferentiated chondritic bodies (Grimm and McSween, 1989; Jewitt et al., 2007; Melosh 2011). The dominant heat source for small bodies in the asteroid belt was likely  $^{26}\text{Al}$  (Grimm and McSween, 1989; MacPherson et al., 1995; Jewitt et al., 2007), which is thought to be the heat source for both aqueous alteration and thermal metamorphism. The short half-life of  $^{26}\text{Al}$  ( $\sim 0.7$  Myr) leaves a relatively short window of time for parent body alteration to occur on small, undifferentiated asteroids. Models of internal parent-body heating have explored temperatures experienced by asteroids of different size (Grimm and McSween, 1989; Jewitt et al., 2007; Fujiya et al., 2013; Sugiura and Fujiya, 2014; Doyle et al., 2015), under the assumption that  $^{26}\text{Al}$  was homogeneously distributed in the solar accretion disk. In the context of models where the chondritic parent body rapidly accreted at  $\sim 3.5$  Myr after CAI formation (Fujiya et al., 2013; Sugiura and Fujiya, 2014), carbonate forming temperatures (between  $\sim 10$  and  $60$  °C; Jilly-Rehak et al., 2015) should have easily been reached within 1 to 2 Myr after accretion on a parent body of radius  $> 20$  km. Earlier accretion times ( $\sim 2$  Myr after CAI) are also valid, as lower alteration temperatures can be obtained in the outer regions of the asteroid. For parent bodies of this scale, the water would be expected to refreeze within another  $\sim 5$ – $20$  Myr, depending on the radius and time of

accretion (Jewitt et al., 2007; Fujiya et al., 2013). This window of time constrains the potential epoch for aqueous alteration via  $^{26}\text{Al}$ -heating.

#### 4.4.2. Late-stage alteration on the CR parent body

The distinct ages of Renazzo dolomite and GRO 95577 calcite indicate that aqueous alteration on the CR parent body was either prolonged, or occurred in stages. The calcite age in GRO 95577 ( $\sim 12$  Myr after CAI formation) requires a late-stage source of heat for liquid water to be stable and drive aqueous alteration. We propose two hypotheses for the late-stage alteration of GRO 95577 carbonates: internal heating on the CR parent body, or impact heating.

If the CR parent body was sufficiently large to sustain temperatures above the triple point for  $\sim 8$  Myr, then carbonate formation may have occurred before water was lost or any remaining water was re-frozen. In the context of an  $^{26}\text{Al}$  heating model where the parent body accreted at 3.5 Myr after CAI formation (Fujiya et al., 2013; Sugiura and Fujiya, 2014), the parent body radius must have been greater than  $\sim 30$  km for the GRO 95577 calcite to have formed at the right temperatures and times. This minimum radius would also require the GRO 95577 lithology to originate from a warmer, wetter region on the interior of the asteroid. To be consistent with  $^{26}\text{Al}$ -heating models (Wakita and Sekiya, 2011; Fujiya et al., 2013; Sugiura and Fujiya, 2014; Wakita et al., 2014; Doyle et al., 2016), carbonate formation in GRO 95577 must have occurred while the parent body was cooling, after it had reached its peak temperature from  $^{26}\text{Al}$  heating. This would imply that the GRO 95577 lithology experienced higher temperatures before cooling to between 10 and 60 °C. If this scenario is correct, then CR carbonate ages should span a continuum from  $\sim 4$  Myr to  $\sim 13$  Myr after CAI formation, reflecting the prolonged era of alteration. Current isotopic data provide no evidence for this, and petrographic studies of GRO 95577 (Weisberg and Huber, 2007; Briani et al., 2013) show no evidence for high temperatures prior to aqueous alteration.

Furthermore, measurements of siderite in GRO 95577 show no evidence for radiogenic  $^{53}\text{Cr}$ , suggesting that alteration was still taking place  $\sim 24$  Myr after CAI formation (Tyra et al., 2010), when the  $^{53}\text{Mn}$  was no longer alive. This scenario would require an even larger parent body radius of  $\geq 50$  km if heating was sustained by  $^{26}\text{Al}$  (Fujiya et al., 2013). An alternate model suggests that an asteroidal parent body that began accretion before  $\sim 1.5$  Myr after CAIs could internally differentiate to create a crust. If such a body were to continue to accrete material past  $\sim 1.5$  Myr, it could have an undifferentiated (i.e., chondritic) crust (Elkins-Tanton et al., 2011; Weiss and Elkins-Tanton, 2013). Such a setting could potentially allow for very late-stage alteration events. However, while the thermal evolution models are highly dependent on a number of important factors (e.g., time of accretion, mass, radius, density, water/rock ratio, extent of fluid flow), the time and temperature conditions for calcite, dolomite, and siderite formation are unlikely to occur in a single parent body heated by  $^{26}\text{Al}$  alone (see models in Wakita and Sekiya, 2011;

Fujiya et al., 2013; Sugiura and Fujiya, 2014; Wakita et al., 2014; Doyle et al., 2016). In addition, there is no evidence of extensively metamorphosed CR chondrites that would be expected in a large body (i.e., type 4, 5, or 6 chondrites). Therefore, an alternative model for heating be invoked to explain the timing and conditions for alteration in CR chondrites.

Heat from impacts may have driven the late-stage aqueous alteration observed in GRO 95577. Models of post-accretional impacts show that the heat from impact can easily melt ice to a depth of several kilometers (Grimm and McSween, 1989), allowing for aqueous alteration to occur sufficiently later than alteration from  $^{26}\text{Al}$ -heating alone. If the impact scenario is correct, then aqueous alteration would have occurred at discrete ages, reflecting the time of impact events large enough to melt ice. Three CR chondrites show extensive evidence of shock (Miller Range (MIL) 07513, Graves Nunataks (GRA) 06100, and GRO 03116), confirming that large impacts occurred on the CR parent body (Abreu, 2012). Raman analyses of organic matter in CR chondrites have shown that GRA 06100 and GRO 03116 experienced higher temperature alteration than other CR chondrites (Briani et al., 2013). They found the organic signatures to be inconsistent with long-duration thermal metamorphism, and likely reflected heating events with strong kinetic effects, consistent with impacts. Impact processes on the CR parent body have also been invoked for the formation of high-temperature alteration products in GRA 06100, along with accessory carbonates and phosphates (Abreu and Bullock, 2013). Though GRA 06100 was not studied here, it would be interesting to measure the carbonates for  $^{53}\text{Mn}$ – $^{53}\text{Cr}$  to determine whether they formed contemporaneously with the GRO 95577 calcites.

Since the measurements here represent the only resolved  $^{53}\text{Mn}$ – $^{53}\text{Cr}$  ages for CR alteration products, it is difficult to distinguish which of the late-stage heating scenarios is correct. Although our data set is still small, the presence of  $\delta^{53}\text{Cr}^*$  in secondary carbonates from CR chondrites indicates a longer and more traceable aqueous history in CR chondrites than other chondrite groups. The large uncertainties may interfere with the ability to resolve distinct alteration events, but these analyses, along with the unresolved analyses in siderite from Tyra et al. (2010), highlight that the CR carbonates preserve a wide range of alteration ages. SIMS techniques are still developing, and may soon be able to measure smaller grains with higher ion yields, resulting in higher precision for future studies. Efforts to determine mineral RSFs for the Mn–Cr system are currently underway (e.g., Steele and McKeegan, 2014; Ichimura and Sugiura, 2015) and will improve the accuracy of measurements as well.

#### 4.5. Comparison of CR carbonate ages to secondary mineral ages in other chondrites

The absolute ages of the Renazzo calcite and dolomite grains are in agreement with carbonates measured in Tagish Lake and CM and CI chondrites (Fig. 12). Most carbonates have absolute ages between 4 and 6 Myr after CAI formation. The filled symbols in Fig. 12 are from this study, and

the open symbols are from the studies of Tyra et al. (2010), Fujiya et al. (2012, 2013), Jilly et al. (2014), and van Kooten et al. (2016). All literature data have been re-calculated by anchoring to the D'Orbigny angrite (McKibbin et al., 2015) and to the CAI age of Bouvier et al. (2011) for consistency (cf. supplementary material). Dolomite is designated by circle symbols, calcite by squares, and siderite by a triangle. We can compare our data to that of Fujiya et al. (2012, 2013), Jilly et al. (2014), and van Kooten et al. (2016), because they used the same matrix-matched synthetic calcite standards as we did in this study, and measured the RSF values independently using the methods, instruments, and conditions of the unknown. The upper limit of the unresolved Tyra et al. (2010) siderite data is added for comparison of carbonates in GRO 95577, even though the same standards were not used. Note the dolomite data in Fujiya et al. (2012, 2013) and van Kooten et al. (2016) were obtained with the calcite standard and the inferred dolomite RSF is not applied to recalculate them, therefore they are most directly comparable to the RSF value of 0.65 for the Renazzo dolomite. The large uncertainties in the measurements in the CR chondrites compared with those in the literature are due to the low count rates for Mn and Cr. The good agreement between carbonate ages in Renazzo and those in other carbonaceous chondrites suggests that rapid alteration after accretion on chondritic parent bodies was common in the early Solar System.

The GRO 95577 calcites are far younger than most other meteoritic carbonates in Fig. 12. The calcites from Renazzo and GRO 95577 are resolved from each other at about the 85% confidence level (or about  $1.7\sigma$ ), while GRO 95577 calcite is fully resolved from the Renazzo dolomite. It should be noted that Fujiya et al. (2013) reported one dolomite grain in Orgueil with no evidence for live  $^{53}\text{Mn}$  at the time of formation, but concluded that the isochron was either disturbed or that the grain had a different origin than the other grains. Similarly, siderite in GRO 95577 measured with the Mn–Cr system showed no evidence for having contained live  $^{53}\text{Mn}$  (Tyra et al. 2010), possibly corroborating late-stage alteration in CR parent body history. The upper limits for these analyses are plotted in Fig. 12.

Some previous  $^{53}\text{Mn}$ – $^{53}\text{Cr}$  studies of carbonates in carbonaceous chondrites are not included in Fig. 12, as they have used silicate mineral or glass standards, or have used RSF values from literature to correct their data (Endreß et al., 1996; Hoppe et al., 2007; De Leuw et al., 2009; Petit et al., 2009, 2011; Blinova et al., 2012; Lee et al., 2012). These silicate RSF values range from 0.93 to 1.08 (or in some cases are not reported), and are much higher than the RSFs determined for carbonates here and in recent literature (Sugiura et al., 2010; Fujiya et al., 2012, 2013; Jilly et al., 2014; Steele and McKeegan, 2014; Ichimura and Sugiura, 2015). The higher RSF overestimates the value of  $(^{53}\text{Mn}/^{55}\text{Mn})_0$ . We therefore urge the reader to take caution when comparing inter-laboratory studies measured with different standards, as even small changes in the RSF can result in differences of millions of years in the inferred age.

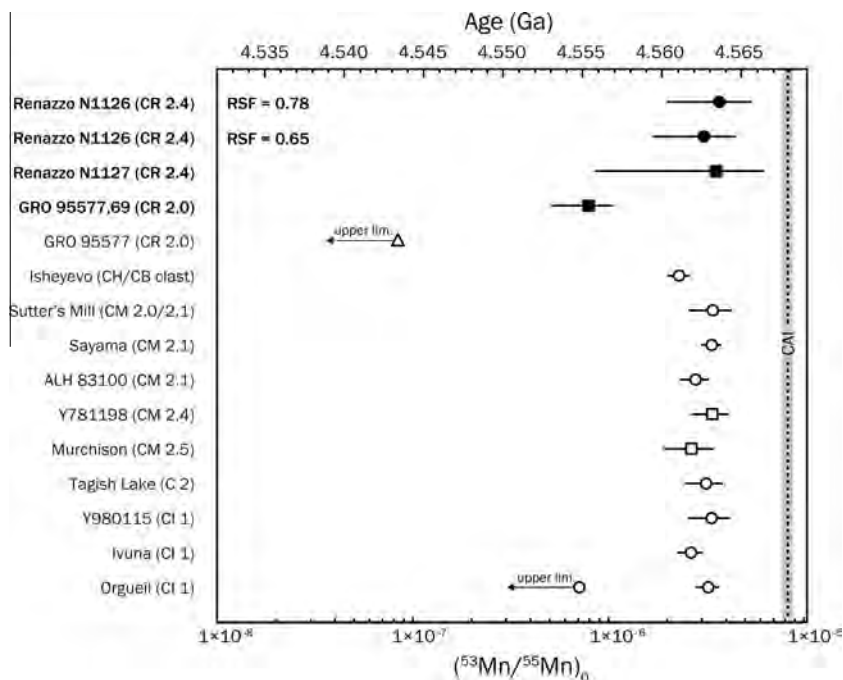


Fig. 12. Absolute ages of carbonates measured by Mn–Cr. The age (Ga) is presented on the top axis, and the corresponding initial  $(^{53}\text{Mn}/^{55}\text{Mn})_0$  is presented on the bottom axis. The filled symbols represent data from this study. Circles represent dolomite analyses, squares represent calcite, and the triangle is siderite. For the Renazzo dolomite, we present data for two different RSF values, since the correction factor is poorly constrained. Renazzo N1127 and GRO 95577 calcites use the boot-strapped RSF value of 0.67. Sutter's Mill datum is from Jilly et al. (2014), Isheyevu datum is from van Kooten et al. (2016). Upper age limits for unresolved siderite in GRO 95577 (Tyra et al., 2010) and dolomite in Orgueil (Fujiya et al., 2013) are indicated with arrows. Remaining data are from Fujiya et al. (2012, 2013). The CAI line represents the CV CAI formation age of  $4567.94 \pm 0.31$  Myr from Bouvier et al. (2011). The Renazzo calcite and dolomite plots contemporaneously with previously measured carbonates in CI and CM chondrites, but GRO 95577 calcites were formed later. Error bars are  $2\sigma$ .

Fayalite is another secondary mineral that has been measured with the Mn–Cr system to provide secondary alteration ages in chondrites. Fayalite grains measured with a matrix-matched standard in ordinary, CV, and CO-like chondrites have ages ranging from  $\sim 2$  to 5 Myr after CAI formation (Doyle et al., 2015, 2016), consistent with the Renazzo calcite and dolomite measured here. These measurements provide further support for the  $^{26}\text{Al}$  heating model for parent body aqueous alteration.

#### 4.6. Potential issues with ages determined by radiometric dating

One main distinction between the CR chondrites and other chondrites may pose a problem for the parent body alteration model. There is significant overlap in the uncertainties in  $^{26}\text{Al}$ – $^{26}\text{Mg}$  CR chondrule ages from literature and our  $^{53}\text{Mn}$ – $^{53}\text{Cr}$  alteration ages (Fig. 13).  $^{26}\text{Al}$ – $^{26}\text{Mg}$  dating of CR chondrules has suggested that they formed later than chondrules from petrologic type 3.0 chondrites. Chondrules from the most primitive CO and UOC chondrites range in age from  $\sim 1$  to 3 Myr after CAI formation (e.g., Kita et al., 2000; Huss et al., 2001; Kurahashi et al., 2008; Kita and Ushikubo, 2012 and references therein), whereas the CR chondrule ages range from  $\sim 1$  to  $\geq 4$  Myr with over 60% of measured CR chondrules show-

ing no resolvable excess of  $^{26}\text{Mg}$  (Nagashima et al., 2007, 2008, 2014; Hutcheon et al., 2009; Kita and Ushikubo, 2012; Schrader et al., 2013b, 2016; Tenner et al., 2015a,b). These Al–Mg ages are calculated assuming that  $(^{26}\text{Al}/^{27}\text{Al})_0$  for CV CAIs represents homogeneous distribution of  $^{26}\text{Al}$  in the protoplanetary disk at the canonical level ( $\sim 5 \times 10^{-5}$ ; e.g. MacPherson et al., 1995; Krot et al., 2006c; Jacobsen et al., 2008). Additionally, Pb–Pb measurements of three CR chondrules by Bollard et al. (2014) yield chondrule ages that span from being contemporaneous with CV CAIs to up to  $\sim 4$  Myr after CAI formation (Fig. 13). One study using the Pb–Pb system found that CR chondrules formed around  $2.5 \pm 1.2$  Myr after CAI formation (Amelin et al., 2002), but has since been recalculated assuming a  $^{238}\text{U}/^{235}\text{U}$  ratio of 137.79 to yield a younger CR chondrule age of  $\sim 4$  Myr after CV CAI formation (Bouvier et al., 2011) that more closely reflects the  $^{26}\text{Al}$ – $^{26}\text{Mg}$  ages (Schrader et al., 2013b; Nagashima et al., 2014). Although the uniform U-isotope composition among chondrules measured to date (Connelly et al., 2012) suggests that this approach is reasonable, a possibility that the chondrules measured by Amelin et al. (2002) have different U-isotope ratios cannot be ruled out, and thus the re-calculated Pb–Pb age may not be reliable.

If the majority of CR chondrules were indeed formed later than 3 or 4 Myr after CAI formation, as given by

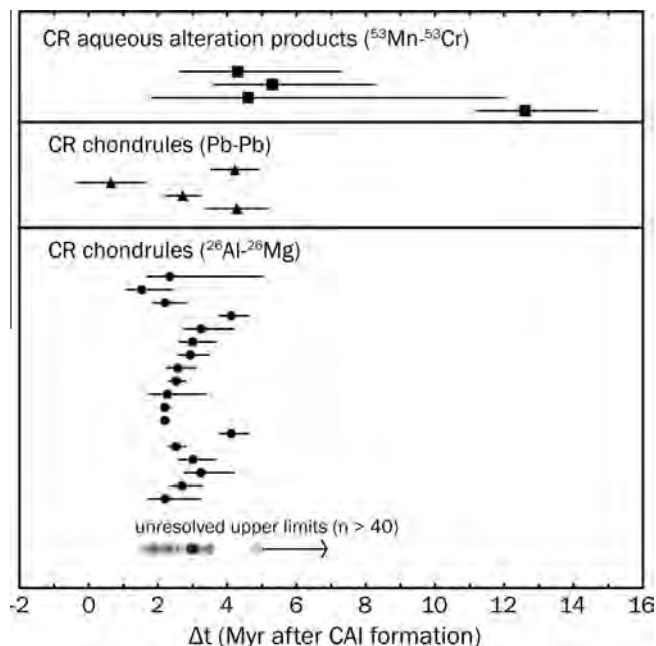


Fig. 13. Comparison between aqueous alteration ages (this study), U-isotope corrected Pb–Pb ages (Amelin et al., 2002; Bollard et al., 2014) and  $^{26}\text{Al}$ – $^{26}\text{Mg}$  chondrule ages from CR chondrites (Hutcheon et al., 2009; Schrader et al., 2013b; Nagashima et al., 2014; Tenner et al., 2015b). Chondrule ages assume canonical  $^{26}\text{Al}/^{27}\text{Al} = 5.23 \times 10^{-5}$  (Jacobsen et al., 2008). Over 40 analyses yielded  $^{26}\text{Al}$ – $^{26}\text{Mg}$  ages unresolved from zero; upper limits for those isochrons are shown as grey circles. CV CAI Pb–Pb age taken as  $4567.94 \pm 0.31$  Myr (Bouvier et al., 2011).

the  $^{26}\text{Al}$ – $^{26}\text{Mg}$  upper limits and late Pb–Pb ages (Amelin et al., 2002; Hutcheon et al., 2009; Kita and Ushikubo, 2012; Schrader et al., 2013b; Bollard et al., 2014; Nagashima et al., 2014; Tenner et al., 2015a), then our  $^{53}\text{Mn}$ – $^{53}\text{Cr}$  data would suggest that subsequent accretion and parent body alteration occurred within a very short timescale, appearing effectively simultaneous within the resolution of the radiochronometers. This effect would be further exacerbated if the Pb–Pb age of CAIs is taken as  $4567.30 \pm 0.16$  Myr (Connelly et al., 2012), rather than  $4567.94 \pm 0.31$  Myr (Bouvier et al., 2011). While large asymmetric uncertainties may be the main reason the relative ages between alteration and chondrule forming events overlap, it is worth delving deeper into this issue to determine if any inconsistencies exist.

To reconcile any potential age issue, we will investigate the following possible scenarios in further detail: (1)  $^{26}\text{Al}$ – $^{26}\text{Mg}$  was heterogeneously distributed in the early Solar System, and a less-than-canonical abundance of  $^{26}\text{Al}$  was incorporated into the CR chondrules, thus providing apparent younger ages (e.g., Bollard et al., 2014, 2015). (2) The  $^{26}\text{Al}$ – $^{26}\text{Mg}$  systematics measured in CR chondrules are disturbed, and do not represent true CR chondrule formation ages. (3) The  $^{53}\text{Mn}$ – $^{53}\text{Cr}$  ages do not represent the true ages of carbonate formation in CR chondrites. (4) The uncertainties in the half-lives of  $^{53}\text{Mn}$  and  $^{26}\text{Al}$  lead to apparent overlapping ages.

The issue of  $^{26}\text{Al}$  homogeneity is controversial, with no clear consensus among the scientific community about whether the live radionuclide was distributed evenly in the solar disk. Some have argued that the inconsistencies

between Pb–Pb ages and  $^{26}\text{Al}$ – $^{26}\text{Mg}$  ages for a number of systems including angrites, CAIs, and chondrules, are due to non-canonical initial abundances of  $^{26}\text{Al}$  in the solar disk (e.g., Larsen et al., 2011; Bollard et al., 2014). The non-canonical abundances are proposed to originate through physical or thermal fractionation of components inherited from the Sun's parent molecular cloud. Alternatively, inconsistencies in the  $^{26}\text{Al}$ – $^{26}\text{Mg}$  system may instead point to Mg-isotope heterogeneity, which can vary independently of Al-isotope distribution (Wasserburg et al., 2012). However, some dispute these claims citing  $^{26}\text{Al}$ – $^{26}\text{Mg}$  analyses that are in agreement with more recent U-isotope corrected Pb–Pb measurements, which would imply a chronological significance (e.g., Schrader et al., 2013b). Support for  $^{26}\text{Al}$  homogeneity also comes from updated initial ratios for the  $^{182}\text{Hf}$ – $^{182}\text{W}$  system, which have now yielded CAI isochrons that are consistent with  $^{26}\text{Al}$ – $^{26}\text{Mg}$  analyses (Kruijer et al., 2014). More coordinated efforts to understand the U–Pb and Al–Mg systems are clearly necessary to determine the consistency of radiometric systems and true relative ages of key processes in the early solar system.

Overlapping CR-chondrule and alteration ages could potentially point to disturbances of the  $^{26}\text{Al}$ – $^{26}\text{Mg}$  dating system. The majority of chondrules that have yielded old  $^{26}\text{Al}$ – $^{26}\text{Mg}$  ages of  $\sim 2$  Myr after CAI formation were from primitive type 3.0, UOC and CO chondrites that have not experienced extensive parent-body aqueous alteration. No chondrules from CM chondrites (all type 1 or 2) have ever been dated using the  $^{26}\text{Al}$ – $^{26}\text{Mg}$  system due to their heavily altered nature. Nearly all CR chondrites are type 2, and have been affected by aqueous alteration to some extent,

while largely avoiding thermal metamorphism. Thermal alteration has been shown to cause Mg diffusion in feldspar at temperatures as low as 400–500 °C (LaTourette and Wasserburg, 1998; Van Orman et al., 2014), but the low-temperature aqueous alteration process has a poorly understood effect on the Al–Mg system.

Recently,  $^{26}\text{Al}$ – $^{26}\text{Mg}$  measurements in chondrule glass and plagioclase have been called into question, particularly for model isochrons where the intercept is forced through the origin (Alexander and Ebel, 2012). There is abundant evidence that chondrule mesostases (where glass and plagioclase reside) can exchange mobile elements with the matrix during low-temperature aqueous processing (c.f. Fig. 9; Burger and Brearley, 2004; Jilly and Huss, 2012). Some low-petrologic-type chondrules also show evidence of O isotopic exchange between the mesostasis and the matrix (Kita et al., 2010). If Mg isotopic exchange occurred to some extent in chondrules while  $^{26}\text{Al}$  was still alive as well, then the ages may partly record the time of alteration, rather than the time of initial formation. However, some chondrule glasses in type 3 ordinary chondrites showed measurable excesses in  $^{26}\text{Mg}$ , despite considerable O isotope exchange (Kita et al., 2010; Alexander and Ebel, 2012). This may be to differences in wet diffusion rates between O and cations; O self-diffusion rates in many silicates are enhanced significantly under wet conditions, while cations in silicates do not show such enhancement (e.g., Farver, 2010 and references therein). Thus O-isotopes may not be good indicators for diffusive redistribution of Mg in aqueously altered samples.

Regardless, this issue does not appear to affect most of the  $^{26}\text{Al}$ – $^{26}\text{Mg}$  measurements for CR chondrites (e.g., Schrader et al., 2013b; Nagashima et al., 2014; Tenner et al., 2015b), which display  $\delta^{26}\text{Mg}^*$  intercepts consistent with zero, and were measured mostly in plagioclase with no evidence for decomposition by aqueous alteration. Furthermore, O isotopes in the CR chondrules measured show no clear evidence for O isotope diffusion (e.g., Krot et al., 2006b; Schrader et al., 2013a, b; Tenner et al., 2015a), supporting the validity of the  $^{26}\text{Al}$ – $^{26}\text{Mg}$  isochrons.

Two issues that could potentially lead to false  $^{53}\text{Mn}$ – $^{53}\text{Cr}$  carbonate ages include isochron disturbances and inaccurate time anchors. Could a disturbance in the  $^{53}\text{Mn}$ – $^{53}\text{Cr}$  system cause the ages of the secondary Renazzo carbonates to appear older than they truly are? Prolonged periods of alteration can disturb the  $^{53}\text{Mn}$ – $^{53}\text{Cr}$  isochron if there is incomplete dissolution and re-precipitation of the carbonates. Such a replacement process would cause the slope of the isochron to become shallower, yielding younger ages of carbonate precipitation that partially reflect the later aqueous processing. Alternatively, the  $^{53}\text{Mn}$ – $^{53}\text{Cr}$  systematics theoretically could have been disturbed towards older ages if Mn was somehow removed from the carbonates after they were formed, without dissolving the carbonates so that they retain  $\delta^{53}\text{Cr}^*$  values greater than zero. The carbonates in Renazzo do not show obvious petrographic or textural evidence such as reaction rims, embayment, or leaching of Mn into the surrounding matrix that would be indicative of such an event, and no resolvable isochron disturbances. However, a detailed

cathodoluminescence study would help to clarify this issue, and determine if multi-stage formation of carbonates occurred. The absolute  $^{53}\text{Mn}$ – $^{53}\text{Cr}$  ages could also be shifted relative to other systems if the D’Orbigny  $^{53}\text{Mn}$ – $^{53}\text{Cr}$  time anchor is incorrect. We discussed the reliability of the D’Orbigny age above (cf., Section 4.3.), and chose a time anchor that is consistent with measurements in the  $^{26}\text{Al}$  system. We therefore do not consider the time anchor likely to be the source of inconsistency.

Lastly, while many of the radiometric systems are internally consistent, the half-lives of the radioactive species are not well constrained. The half-life for  $^{26}\text{Al}$  is inconsistently referenced in the literature, with values ranging from 705,000 to 730,000 years (e.g., Norris et al., 1983; Russell et al., 1994; Jacobsen et al., 2008; Hutcheon et al., 2009; Kita and Ushikubo, 2012; Schrader et al., 2016b). A shorter half-life for  $^{26}\text{Al}$  would pull the chondrules away from the  $^{53}\text{Mn}$ – $^{53}\text{Cr}$  carbonate ages in time. Some papers have also cited a half-life of 3.8 Myr for the  $^{53}\text{Mn}$  (Norris et al., 1983), rather than the 3.7 Myr value (Honda and Imamura, 1971) used here. Using the shorter  $^{26}\text{Al}$  half-life would cause a  $\sim 3.5\%$  difference in the chondrule ages, and the longer  $^{53}\text{Mn}$  half-life shifts the carbonate ages by  $\sim 3\%$ . Even together, using these different half-lives cannot solve the problem and resolve the chondrule-forming and aqueous alteration events.

The scenarios presented above demonstrate that there is still significant work to be done in clarifying inconsistencies among the different radiometric dating methods. The simplest explanation for the overlapping CR chondrule age and aqueous alteration age is that the uncertainties are currently too large to resolve the specific events with sufficient accuracy. Many open questions remain regarding absolute timescales in the early solar system history, though this work demonstrates that CR chondrule formation, accretion, and the onset of aqueous alteration likely occurred in rapid succession. Despite the clear need for more precise and accurate measurements, the relative  $^{53}\text{Mn}$ – $^{53}\text{Cr}$  carbonate ages provide invaluable constraints on the prolonged duration of aqueous alteration on the CR parent body.

## 5. CONCLUSIONS

We measured carbonates in the CR chondrites Renazzo and GRO 95577 for  $^{53}\text{Mn}$ – $^{53}\text{Cr}$ . Both dolomite and calcite show clear excesses of  $^{53}\text{Cr}$ , interpreted as the daughter product of  $^{53}\text{Mn}$  decay. The Renazzo calcite grains have an alteration age of  $4.6^{+7.4}_{-2.8}$  Myr after the formation of CAI, and Renazzo dolomite alteration ages are  $5.3^{+3.0}_{-1.7}$  or  $4.3^{+3.0}_{-1.7}$  Myr after CAI for the RSF values of 0.65 and 0.78, respectively. GRO 95577 calcite was younger, formed  $12.6^{+2.1}_{-1.4}$  Myr after CAI. The distinct ages suggest that aqueous alteration on the CR parent body did not occur in one instance, but instead was prolonged or occurred in stages. These data indicate that the calcite and dolomite in Renazzo formed during aqueous alteration early in the history of the CR parent body, likely as a consequence of internal heating from  $^{26}\text{Al}$  decay. For the carbonates in GRO 95577 to have been formed so late and at cool temperatures of 10–60 °C (Jilly-Rehak et al.,

2015), either the parent body was sufficiently large (at least 30–50 km radius) to retain enough heat, or late-stage impact events supplied heat to the GRO 95577 lithology. In the late-stage  $^{26}\text{Al}$ -decay heating scenario, GRO 95577 likely originated from a warmer, wetter region on the interior of the asteroid, and aqueous alteration would have had to occur as the parent body was cooling down after the initial rapid heating from  $^{26}\text{Al}$ . More likely, an impact-heating scenario resulted in the formation of the calcites, where the GRO 95577 lithology would have originated from a shallower depth that was heated substantially by shock. Our research has provided answers to key questions about the timing of aqueous alteration for the CR chondrites, and it also provides direction for future studies to better resolve events in the history of CR chondrites.

#### ACKNOWLEDGEMENTS

This work was supported by NASA Headquarters under the NASA Earth and Space Science Fellowship Program – Grant NNX14AO29H (C. E. Jilly-Rehak), as well as NASA Cosmochemistry grants NNX11AG78G and NNX14AI19G (G. R. Huss, PI), and NAI cooperative agreement NNA04CC08A (K. Meech, PI). We thank the Johnson Space Center's Meteorite Working Group and the Museum of Natural History Vienna for providing the meteorite samples and for the special thin section preparations. This manuscript was significantly improved by the thoughtful revisions from S. McKibbin, S. Mostefaoui, and M. Tyra. Additionally, this work benefitted from discussions and assistance from the following researchers: T. Doyle, K. Ichimura, R. Oglione, D. Schrader, R. Steele, M. Telus, and A. Thomen. This is Hawaii Institute of Geophysics and Planetology publication #2225, and School of Ocean and Earth Science and Technology publication #9816.

#### APPENDIX A. SUPPLEMENTARY DATA

Supplementary data associated with this article can be found, in the online version, at <http://dx.doi.org/10.1016/j.gca.2016.08.033>.

#### REFERENCES

- Abreu N. M. (2012) CR chondrites: shock, aqueous alteration and terrestrial weathering. *AGU Fall Meeting Abstracts*, #1909 (abstr.).
- Abreu N. M. and Brearley A. J. (2005) Carbonates in vigarano: terrestrial, preterrestrial, or both? *Meteorit. Planet. Sci.* **40**, 609–625.
- Abreu N. M. and Brearley A. J. (2010) Early solar system processes recorded in the matrices of two highly pristine CR3 carbonaceous chondrites, MET 00426 and QUE 99177. *Geochim. Cosmochim. Acta* **74**, 1146–1171.
- Abreu N. M. and Bullock E. S. (2013) Opaque assemblages in CR2 Graves Nunataks (GRA) 06100 as indicators of shock-driven hydrothermal alteration in the CR chondrite parent body. *Meteorit. Planet. Sci.* **48**, 2406–2429.
- Alexander C. M. O. D. and Ebel D. S. (2012) Questions, questions: can the contradictions between the petrologic, isotopic, thermodynamic, and astrophysical constraints on chondrule formation be resolved? *Meteorit. Planet. Sci.* **47**, 1157–1175.
- Amelin Y. (2008) U–Pb ages of angrites. *Geochim. Cosmochim. Acta* **72**, 221–232.
- Amelin Y., Krot A. N., Hutcheon I. D. and Ulyanov A. A. (2002) Pb isotopic ages of chondrules and Ca–Al-rich inclusions. *Science* **297**, 1678–1683.
- Amelin Y., Kaltenbach A., Iizuka T., Stirling C. H., Ireland T. R., Petaev M. and Jacobsen S. B. (2010) U–Pb chronology of the Solar System's oldest solids with variable  $^{238}\text{U}/^{235}\text{U}$ . *Earth Planet. Sci. Lett.* **300**, 343–350.
- Astafieva M. M., Rozanov A. Y. and Hoover R. B. (2004) Framboidal structures in Earth rocks and in astromaterials. *Proc. SPIE* **5163**, 36–47.
- Benedix G. K., Leshin L. A., Farquhar J., Jackson T. and Thiemens M. H. (2003) Carbonates in CM2 chondrites: constraints on alteration conditions from O isotopic compositions and petrographic observations. *Geochim. Cosmochim. Acta* **67**, 1577–1588.
- Birck J. L. and Allègre C. J. (1984) Cr isotopic anomalies in Allende Refractory Inclusions. *Geophys. Res. Lett.* **10**, 943–946.
- Birck J. L., Rotaru M. and Allègre C. J. (1999)  $^{53}\text{Mn}$ – $^{53}\text{Cr}$  evolution of the early Solar System. *Geochim. Cosmochim. Acta* **63**, 4111–4117.
- Bland P. A., Zolensky M. E., Benedix G. K. and Sephton M. A. (2006) Weathering of chondritic meteorites. In *Meteorites and the Early Solar System II* (eds. D. S. Lauretta and H. Y. McSween). University of Arizona Press, Tucson, pp. 853–867.
- Bland P. A., Jackson M. D., Coker R. F., Cohen B. A., Webber J. B. W., Lee M. R., Duffy C. M., Chater R. J., Ardakani M. G., McPhail D. S., McComb D. W. and Benedix G. K. (2009) Why aqueous alteration in asteroids was isochemical: high porosity  $\neq$  high permeability. *Earth Planet. Sci. Lett.* **287**, 559–568.
- Blinova A., Alexander C. M. O'D., Wang J. and Herd C. D. K. (2012) Mineralogy and Mn–Cr extinct radionuclide dating of a dolomite from the pristine Tagish Lake meteorite. *Lunar Planet. Sci. XLIII*, #1188 (abstr.).
- Bollard J., Connelly J. N., and Mizzarro M. (2014) The absolute chronology of the early solar system revisited. *77th Annual Meeting of the Meteoritical Society*, #5234 (abstr.).
- Bollard J., Kawasaki N., Sakamoto N., Larsen K., Wielandt D., Schiller M., Connelly J., Yurimoto H., and Bizzarro M. (2015) Early disk dynamics inferred from isotope systematics of individual chondrules. *78th Annual Meeting of the Meteoritical Society*, #5211 (abstr.).
- Bouvier A. and Wadhwa M. (2010) The age of the Solar System redefined by the oldest Pb–Pb age of a meteoritic inclusion. *Nat. Geosci.* **3**, 637–641.
- Bouvier A., Brennecka G. A. and Wadhwa A. (2011) Absolute chronology of the first solids in the solar system. *Workshop on the formation of the first solids in the solar system, Kauai*, #9054 (abstr.).
- Brearley A. J. (2006) The Action of Water. In *Meteorites and the Early Solar System II* (eds. D. S. Lauretta and H. Y. McSween). University of Arizona Press, Tucson, pp. 584–624.
- Brennecka G. A. and Wadhwa M. (2012) U isotope compositions of the basaltic angrite meteorites and the chronological implications for the early Solar System. *Proc. Natl. Acad. Sci. USA* **109**, 9299–9303.
- Briani G., Quirico E., Gounelle M., Paulhiac-Pison M., Montagnac G., Beck P., Orthous-Daunay F.-R., Bonal L., Jacquet E., Kearsley A. and Russell S. S. (2013) Short duration thermal metamorphism in CR chondrites. *Geochim. Cosmochim. Acta* **122**, 267–279.
- Browning L. B., McSween H. Y. and Zolensky M. E. (1996) Correlated alteration effects in CM carbonaceous chondrites. *Geochim. Cosmochim. Acta* **60**, 2621–2633.

- Burger P. V. and Brearley A. J. (2004) Chondrule glass alteration in type IIA chondrules in the CR2 chondrites EET 87770 and EET 92105: Insights into elemental exchange between chondrules and matrices. *Lunar Planet. Sci. XXXV*, #1966 (abstr.).
- Ciesla F. J., Lauretta D. S., Cohen B. A. and Hood L. L. (2003) A Nebular origin for chondritic fine-grained phyllosilicates. *Science* **299**, 549–552.
- Clayton R. N. and Mayeda T. K. (1977) O isotopic compositions of separated fractions of the Leoville and Renazzo carbonaceous chondrites. *Meteoritics* **12**, A199.
- Clayton R. N. and Mayeda T. K. (1984) The O isotope record in Murchison and other carbonaceous chondrites. *Earth Planet. Sci. Lett.* **67**, 151–161.
- Clayton R. N. and Mayeda T. K. (1999) O isotope studies of carbonaceous chondrites. *Geochim. Cosmochim. Acta* **63**, 2089–2104.
- Cohen B. A. and Coker R. F. (2000) Modeling of liquid water on CM meteorite parent bodies and implications for amino acid racemization. *Icarus* **145**, 369–381.
- Connelly J. N., Bizzarro M., Krot A. N., Nordlund A., Wielandt D. and Ivanova M. A. (2012) The absolute chronology and thermal processing of solids in the solar protoplanetary disk. *Science* **338**, 651–655.
- Cyr K. E., Sears W. D. and Lunine J. I. (1998) Distribution an evolution of water ice in the solar nebula: Implications for Solar System body formation. *Icarus* **135**, 537–548.
- De Leuw S., Rubin A. E., Schmitt A. K. and Wasson J. T. (2009)  $^{53}\text{Mn}$ – $^{53}\text{Cr}$  systematics of carbonates in CM chondrites: Implications for the timing and duration of aqueous alteration. *Geochim. Cosmochim. Acta* **73**, 7433–7442.
- Doyle P. M., Jogo K., Nagashima K., Krot A. N., Wakita S., Ciesla F. and Hutcheon I. D. (2015) Early aqueous activity on the ordinary and carbonaceous chondrite parent bodies recorded by fayalite. *Nat. Commun.* **6**, 7444.
- Doyle P. M., Jogo K., Nagashima K., Huss G. R. and Krot A. N. (2016) Mn–Cr relative sensitivity factor in ferromagnesian olivines defined for SIMS measurements with a Cameca ims-1280 ion microprobe: Implications for dating secondary fayalite. *Geochim. Cosmochim. Acta* **174**, 102–121.
- Elkins-Tanton L. T., Weiss B. P. and Zuber M. T. (2011) Chondrites as samples of differentiated planetesimals. *Earth Planet. Sci. Lett.* **305**, 1–10.
- Endreß M. and Bischoff A. (1996) Carbonates in CI chondrites: clues to parent body evolution. *Geochim. Cosmochim. Acta* **60**, 489–507.
- Endreß M., Zinner E. and Bischoff A. (1996) Early aqueous activity on primitive meteorite parent bodies. *Nature* **379**, 701–703.
- Farver J. R. (2010) O and hydrogen diffusion in minerals. *Rev. Mineral. Geochem.* **72**, 447–507.
- Fujiya W., Sugiura N., Hotta H., Ichimura K. and Sano Y. (2012) Evidence for the late formation of hydrous asteroids from young meteoritic carbonates. *Nat. Commun.* **3**, 627.
- Fujiya W., Sugiura N., Sano Y. and Hiyagon H. (2013) Mn–Cr ages of dolomites in CI chondrites and the Tagish Lake ungrouped carbonaceous chondrite. *Earth Planet. Sci. Lett.* **362**, 130–142.
- Glavin D. P., Kubny A., Jagoutz E. and Lugmair G. W. (2004) Mn–Cr isotope systematics of the D'Orbigny angrite. *Meteorit. Planet. Sci.* **39**, 693–700.
- Grimm R. E. and McSween H. Y. (1989) Water and the thermal evolution of carbonaceous chondrite parent bodies. *Icarus* **82**, 244–280.
- Harju E. R., Rubin A. E., Ahn I., Choi B.-G., Ziegler K. and Wasson J. T. (2014) Progressive aqueous alteration of CR carbonaceous chondrites. *Geochim. Cosmochim. Acta* **139**, 267–292.
- Honda M. and Imamura M. (1971) Half-life of  $^{53}\text{Mn}$ . *Phys. Rev. C* **4**, 1182–1188.
- Hoppe P., MacDougall D. and Lugmair G. W. (2007) High spatial resolution ion microprobe measurements refine chronology of carbonate formation in Orgueil. *Meteorit. Planet. Sci.* **42**, 1309–1320.
- Hua X., Huss G. R., Tachibana S. and Sharp T. G. (2005) O, Si, and Mn–Cr isotopes of fayalite in the Kaba oxidized CV3 chondrite: constraints for its formation history. *Geochim. Cosmochim. Acta* **69**, 1333–1348.
- Huss G. R., MacPherson G. J., Wasserburg G. J., Russell S. S. and Srinivasan G. (2001) Al-26 in Ca–Al-rich inclusions and chondrules from unequilibrated ordinary chondrites. *Meteorit. Planet. Sci.* **36**, 975–997.
- Hutcheon I. D., Krot A. N., Keil K., Phinney D. L. and Scott E. R. D. (1998)  $^{53}\text{Mn}$ – $^{53}\text{Cr}$  dating of fayalite formation in the CV3 chondrites Mokoia: evidence for asteroidal alteration. *Science* **282**, 1865–1867.
- Hutcheon I. D., Marhas K. K., Krot A. N., Goswami J. N. and Jones R. H. (2009)  $^{26}\text{Al}$  in plagioclase-rich chondrules in carbonaceous chondrites: evidence for an extended duration of chondrule formation. *Geochim. Cosmochim. Acta* **73**, 5080–5099.
- Ichikawa O. and Ikeda Y. (1995) Petrology of the Yamato-8449 CR chondrite. *Proc. NIPR. Symp. Antarctic Met.* **8**, 63–78.
- Ichimura K. and Sugiura N. (2015) Preparation of synthetic dolomite for determination of Mn/Cr relative sensitivity. *Lunar Planet. Sci. XLVI*, #1795 (abstr.).
- Ikeda Y. and Prinz M. (1993) Petrologic study of the Belgica 7904 carbonaceous chondrite: hydrous alteration, O isotopes, and relationship to CM and CI chondrites. *Geochim. Cosmochim. Acta* **57**, 439–452.
- Jacobsen B., Yin Q.-Z., Moynier F., Amelin Y., Krot A. N., Nagashima K., Hutcheon I. D. and Palme H. (2008)  $^{26}\text{Al}$ – $^{26}\text{Mg}$  and  $^{207}\text{Pb}$ – $^{208}\text{Pb}$  systematics of Allende CAIs: canonical solar initial  $^{26}\text{Al}/^{27}\text{Al}$  ratio reinstated. *Earth Planet. Sci. Lett.* **272**, 353–364.
- Jewitt D., Chizmadia L., Grimm R., and Prialnik D. (2007) Water in the small bodies of the Solar System. *Protostars and Planets V*, pp. 863–878.
- Jilly C. E. and Huss G. R. (2012) Heterogeneous aqueous alteration in the CR2 chondrite Renazzo. *Lunar Planet. Sci. XLIII*, #1348 (abstr.).
- Jilly C. E., Huss G. R., Krot A. N., Nagashima K., Yin Q.-Z. and Sugiura N. (2014)  $^{53}\text{Mn}$ – $^{53}\text{Cr}$  dating of aqueously formed carbonates in the CM2 lithology of the Sutter's Mill carbonaceous chondrite. *Meteorit. Planet. Sci.* **49**, 2104–2117.
- Jilly-Rehak C. E., Huss G. R. and Nagashima K. (2015) O isotopes in secondary minerals in CR chondrites: Comparing components of different petrologic type. *Lunar Planet. Sci. XLVI*, #1662 (abstr.).
- Jogo K., Nakamura T., Noguchi T. and Zolotov M. Y. (2009) Fayalite in the vigarano CV3 carbonaceous chondrite: occurrences, formation age and conditions. *Earth Planet. Sci. Lett.* **287**, 320–328.
- Kallemeyn G. W., Rubin A. E. and Wasson J. T. (1994) The compositional classification of chondrites: VI. The CR carbonaceous chondrite group. *Geochim. Cosmochim. Acta* **58**, 2873–2888.
- Keil K. (2012) Angrites, a small but diverse suite of ancient, silica-undersaturated volcanic-plutonic mafic meteorites, and the history of their parent asteroid. *Chem. Erde* **72**, 191–218.
- Kita N. T. and Ushikubo T. (2012) Evolution of protoplanetary disk inferred from  $^{26}\text{Al}$  chronology of individual chondrules. *Meteorit. Planet. Sci.* **47**, 1108–1119.

- Kita N. T., Nagahara H., Togashi S. and Morishita Y. (2000) A short duration of chondrule formation in the solar nebula: evidence from  $^{26}\text{Al}$  in Semarkona ferromagnesian chondrules. *Geochim. Cosmochim. Acta* **64**, 3913–3922.
- Kita N. T., Nagahara H., Tachibana S., Tomomura S., Spicuzza M. J., Fournelle J. H. and Valley J. W. (2010) High precision SIMS O three isotope study of chondrules in LL3 chondrites: role of ambient gas during chondrule formation. *Geochim. Cosmochim. Acta* **74**, 6610–6635.
- Kleine T., Hans U., Irving A. J. and Bourdon B. (2012) Chronology of the angrite parent body and implications for core formation in protoplanets. *Geochim. Cosmochim. Acta* **84**, 186–203.
- Krot A. N., Hutcheon I. D., Brearley A. J., Pravdivtseva O. V., Petaev M. I., Hohenberg C. M. (2006a) Timescales and settings for alteration of chondritic meteorites. *Meteorites and the Early Solar System II*. pp. 525–553.
- Krot A. N., Libourel G. and Chaussidon M. (2006b) O isotope compositions of chondrules in CR chondrites. *Geochim. Cosmochim. Acta* **70**, 767–779.
- Krot A. N., McKeegan K. D., Huss G. R., Liffman K., Sahijpal S., Hutcheon I. D., Srinivasan G., Bischoff A. and Keil K. (2006c) Al–Mg and O isotope study of relict Ca–Al rich inclusions in chondrules. *Astrophys. J.* **639**, 1227–1237.
- Kruijer T. S., Kleine T., Fischer-Gödde M., Brukhardt C. and Wieler R. (2014) Nucleosynthetic W isotope anomalies and the Hf–W chronometry of Ca–Al-rich inclusions. *Earth Planet. Sci. Lett.* **403**, 317–327.
- Kurahashi E., Kita N. T., Nagahara H. and ad Morishita Y. (2008)  $^{26}\text{Al}$ – $^{26}\text{Mg}$  systematics of chondrules in a primitive CO chondrite. *Geochim. Cosmochim. Acta* **72**, 3865–3882.
- Larsen K. K., Trinquier A., Paton C., Schiller M., Wielandt D., Ivanova M. A., Connelly J. N., Nordlund Å., Krot A. N. and Bizzarro M. (2011) Evidence for Mg isotope heterogeneity in the solar protoplanetary disk. *Astrophys. J.* **735**, L37.
- LaTourette T. and Wasserburg G. J. (1998) Mg diffusion in anorthite: implications for the formation of early solar system planetesimals. *Earth Planet. Sci. Lett.* **158**, 91–108.
- Lee M. R., Lindgren P., Sofe M. R., Alexander C. M. O'D. and Wang J. (2012) Extended chronologies of aqueous alteration in the CM2 carbonaceous chondrites: evidence from carbonates in Queen Alexandra Range 93005. *Geochim. Cosmochim. Acta* **92**, 148–169.
- Lugmair G. W. and Shukolyukov A. (1998) Early solar system timescales according to  $^{53}\text{Mn}$ – $^{53}\text{Cr}$  systematics. *Geochim. Cosmochim. Acta* **62**, 2863–2886.
- MacPherson G. J., Davis A. M. and Zinner E. K. (1995) The distribution of Al-26 in the early Solar System – a reappraisal. *Meteoritics* **30**, 365–386.
- McKibbin S. J., Ireland T. R., Amelin Y., O'Neill H. S. O. and Holden P. (2013) Mn–Cr relative sensitivity factors for secondary ion mass spectrometry analysis of Mg–Fe–Ca olivine and implications for the Mn–Cr chronology of meteorites. *Geochim. Cosmochim. Acta* **110**, 216–228.
- McKibbin S. J., Ireland T. R., Amelin Y. and Holden P. (2015) Mn–Cr dating of Fe- and Ca-rich olivine from ‘quenched’ and ‘plutonic’ angrite meteorites using Secondary Ion Mass Spectrometry. *Geochim. Cosmochim. Acta* **157**, 13–27.
- McSween, Jr., H. Y. (1979) Alteration in CM carbonaceous chondrites inferred from modal and chemical variations in matrix. *Geochim. Cosmochim. Acta* **43**, 1761–1770.
- Melosh H. J. (2011). , p. 113. Planetary surface processes.
- Mittlefehldt D. W., Killgore M. and Lee M. T. (2002) Petrology and geochemistry of D'Orbigny, geochemistry of Sahara 99555, and the origin of angrites. *Meteorit. Planet. Sci.* **37**, 345–369.
- Nagashima K., Krot A. N. and Chaussidon M. (2007) Al–Mg isotope systematics of chondrules from CR chondrites. *Meteorit. Planet. Sci.* **42**, A115 (abstr.).
- Nagashima K., Krot A. N. and Huss G. R. (2008)  $^{26}\text{Al}$  in chondrules from CR carbonaceous chondrites. *Lunar Planet. Sci. XXXIX*, #2224 (abstr.).
- Nagashima K., Krot A. N. and Huss G. R. (2014)  $^{26}\text{Al}$  in chondrules from CR2 chondrites. *Geochim. J.* **48**, 561–570.
- Norris T. L., Gancarz A. J., Rokop D. J. and Thomas K. W. (1983) Half-life of  $^{26}\text{Al}$ . *J. Geophys. Res.* **88**, B331–B333.
- Nyquist L. E., Lindstrom D., Mittlefehldt D., Shih C.-Y., Wiesmann H., Wentworth S. and Martinez R. (2001) Mn–Cr formation intervals for chondrules from the Bishunpur and Chainpur meteorites. *Meteorit. Planet. Sci.* **36**, 911–938.
- Nyquist L. E., Kleine T., Shih C.-Y. and Reese Y. D. (2009) The distribution of short-lived radioisotopes in the early solar system and the chronology of asteroid accretion, differentiation, and secondary mineralization. *Geochim. Cosmochim. Acta* **73**, 5115–5136.
- Ogliore R. C., Huss G. R. and Nagashima K. (2011) Ratio estimation in SIMS analysis. *Nucl. Instrum. Methods B* **269**, 1910–1918.
- Papanastassiou D. A. (1986) Cr isotopic anomalies in the Allende meteorite. *Astrophys. J.* **308**, L27–L30.
- Papanastassiou D. A., Wasserburg G. J. and Bogdanovski O. (2005) The  $^{53}\text{Mn}$ – $^{53}\text{Cr}$  system in CAIs: An update. *Lunar Planet. Sci. XXXVI*, #2198 (abstr.).
- Petit M., McKeegan K., Gounelle M., Mostefaoui S., Marrocchi Y., Meibom A. and Leshin L. A. (2009) Duration and sequence of carbonate crystallization on the Orgueil protolith:  $^{53}\text{Mn}$ – $^{53}\text{Cr}$  systematics of their evolution in O and C isotopic evolution. *Lunar Planet. Sci. IX*, #1288 (abstr.).
- Petit M., Marrocchi Y., McKeegan K. D., Mostefaoui S., Meibom A., Zolensky M. E. and Gounelle M. (2011)  $^{53}\text{Mn}$ – $^{53}\text{Cr}$  ages of Kaidun carbonates. *Meteorit. Planet. Sci.* **46**, 275–283.
- Russell S. S., Srinivasan G., Huss G. R., Wasserburg G. J. and MacPherson G. J. (1994) Evidence for widespread  $^{26}\text{Al}$  in the Solar Nebula and constraints for nebula time scales. *Science* **273**, 757.
- Sawlowicz Z. (2000) Framboids: From their origin to application. *Pr. Mineral.* **88**, 1–58.
- Schiller M., Baker J. A. and Bizzarro M. (2010)  $^{26}\text{Al}$ – $^{26}\text{Mg}$  dating of asteroidal magmatism in the young Solar System. *Geochim. Cosmochim. Acta* **74**, 4844–4864.
- Schrader D. L., Franchi I. A., Connolly H. C., Greenwood R. C., Lauretta D. S. and Gibson J. M. (2011) The formation and alteration of the Renazzo-like carbonaceous chondrites I: implications of bulk-O isotopic composition. *Geochim. Cosmochim. Acta* **75**, 308–325.
- Schrader D. L., Connolly H. C., Lauretta D. S., Nagashima K., Huss G. R., Davidson J. and Domanik K. J. (2013a) The formation of the Renazzo-like carbonaceous chondrites II: linking O-isotope composition and oxidation state of chondrule olivine. *Geochim. Cosmochim. Acta* **101**, 302–327.
- Schrader D. L., Nagashima K., Krot A. N., Oglione R. C., Yin Q.-Z., and Amelin Y. (2013b) Testing the distribution of  $^{26}\text{Al}$  in the protoplanetary disk using CR chondrules. *76th Annual Meteoritical Society Meeting*, #5141 (abstr.).
- Schrader D. L., Davidson J., Greenwood R. C., Franchi I. A. and Gibson J. M. (2014) A water-ice rich minor body from the early Solar System: the CR chondrite parent asteroid. *Earth Planet. Sci. Lett.* **407**, 48–60.
- Schrader D. L., Nagashima K., Krot A. N., Oglione R. C., Yin Q.-Z., Amelin Y., Striling C. H. and Kaltenbach A. (2016) Distribution of  $^{26}\text{Al}$  in the CR chondrule-forming region of the

- protoplanetary disk. *Geochim. Cosmochim. Acta*. <http://dx.doi.org/10.1016/j.gca.2016.06.023>.
- Shukolyukov A. and Lugmair G. (2006) Mn–Cr isotope systematics of carbonaceous chondrites. *Earth Planet. Sci. Lett.* **250**, 200–213.
- Spandler C., O'Neill H. and St C. (2010) Diffusion and partition coefficients of minor and trace elements in San Carlos olivine at 1,300 °C with some geochemical implications. *Contrib. Mineral. Petrol.* **159**, 791–818.
- Spivak-Birndorf L., Wadhwa M. and Janney P. E. (2009)  $^{26}\text{Al}$ – $^{26}\text{Mg}$  systematics in D'Orbigny and Sahara 99555 angrites: implications for high-resolution chronology using extinct chronometers. *Geochim. Cosmochim. Acta* **73**, 5202–5211.
- Steele R. C. J. and McKeegan K. D. (2014) Aqueous alteration on the CI parent body: Mn–Cr ages of secondary carbonate formation. *The 77th Annual Meteoritical Society Meeting*, #5438 (abstr.).
- Sugiura N., Ichimura K., Fujiya W. and Takahata N. (2010) Mn/Cr relative sensitivity factors for synthetic Ca carbonate measured with a NanoSIMS ion microprobe. *Geochem. J.* **44**, e11–e16.
- Sugiura N. and Fujiya W. (2014) Correlated accretion ages and  $\epsilon^{54}\text{Cr}$  of meteorite parent bodies and the evolution of the solar nebula. *Meteorit. Planet. Sci.* **49**, 772–787.
- Tenner T. J., Nakashima D., Ushikubo T., Kita N. T. and Weisberg M. K. (2015a) O isotope ratios of FeO-poor chondrules in CR3 chondrites: Influence of dust enrichment and  $\text{H}_2\text{O}$  during chondrule formation. *Geochim. Cosmochim. Acta* **148**, 228–250.
- Tenner T. J., Nakashima D., Ushikubo T., Weisberg M. K., and Kita N. T. (2015b) SIMS Al–Mg chronology of CR chondrite chondrules: Links with Mg# and O isotopes. *78th Annual Meeting of the Meteoritical Society*, #5325 (abstr.).
- Trinquier A., Birck J.-L., Allègre C. J., Göpel C. and Ulfbeck D. (2008)  $^{53}\text{Mn}$ – $^{53}\text{Cr}$  systematics of the early Solar System revisited. *Geochim. Cosmochim. Acta* **72**, 5146–5163.
- Tyra M. A., Brearley A. J., Matzel J. and Hutcheon I. D. (2010) Types and timescales of secondary carbonates in CR1 chondrite GRO 95577. *Lunar Planet. Sci. XLI*, #2614 (abstr.).
- Tyra M. A., Brearley A. J. and Guan Y. (2011) O isotopic composition of secondary carbonates in CR1 chondrite GRO 95577. *Lunar Planet. Sci. XLII*, #1639 (abstr.).
- van Kooten E. M. M. E., Wielandt D., Schiller M., Nagashima K., Thomen A., Larsen K. K., Olsen M. B., Nordlund Å., Krot A. N. and Bizarro M. (2016) Isotopic evidence for primordial molecular cloud material in metal-rich carbonaceous chondrites. *Proc. Natl. Acad. Sci.* <http://dx.doi.org/10.1073/pnas.1518183113>.
- Van Orman J. A., Cherniak D. J. and Kita N. T. (2014) Magnesium diffusion in plagioclase: Dependence on composition, and implications for thermal resetting of the  $^{26}\text{Al}$ – $^{26}\text{Mg}$  early solar system chronometer. *Earth Planet. Sci. Lett.* **385**, 79–88.
- Wakita S. and Sekiya M. (2011) Thermal evolution of icy planetesimals in the solar nebula. *Earth Planets Space* **63**, 1193–1206.
- Wakita S., Nakamura T., Ikeda T. and Yurimoto H. (2014) Thermal modeling for a parent body of Itokawa. *Meteorit. Planet. Sci.* **49**, 228–236.
- Wasserburg G. J., Wimpenny J. and Yin Q.-Z. (2012) Mg isotopic heterogeneity, Al–Mg isochrons, and canonical  $^{26}\text{Al}/^{27}\text{Al}$  in the early solar system. *Meteorit. Planet. Sci.* **47**, 1980–1997.
- Weisberg M. K. and Huber H. (2007) The GRO 95577 CR1 chondrite and hydration of the CR parent body. *Meteorit. Planet. Sci.* **42**, 1495–1503.
- Weisberg M. K. and Prinz M. (1998) Fayalitic olivine in CV3 chondrite matrix and dark inclusions: A nebular origin. *Meteorit. Planet. Sci.* **33**, 1087–1099.
- Weisberg M. K., Prinz M., Clayton R. N. and Mayeda T. K. (1993) The CR (Renazzo-type) carbonaceous chondrite group and its implications. *Geochim. Cosmochim. Acta* **57**, 1567–1586.
- Weiss B. P. and Elkins-Tanton L. T. (2013) Differentiates planetesimals and the parent bodies of chondrites. *Annu. Rev. Earth Planet. Sci.* **41**, 529–560.
- Zhukova I., O'Neill H. St. C., and Cambell I. H. (2014a) The effect of mineral paragenesis on Al diffusion in olivine. *EGU General Assembly Abstracts* 16, 573. (abstr.).
- Zhukova I., O'Neill H., St C., Cambell I. H. and Kilburn M. R. (2014b) The effect of silica activity on the diffusion of Ni and Co in olivine. *Contrib. Mineral. Petrol.* **168**, 1029.

Associate editor: Trevor Ireland